

A guide to comprehensive phosphor discovery for solid-state lighting

Shruti Hariyani ^{® 1,2} ⋈, Małgorzata Sójka ^{® 1,2}, Anant Setlur³ & Jakoah Brgoch ^{® 1,2} ⋈

Abstract

Inorganic phosphors have been crucial in enabling energy-efficient, phosphor-converted light-emitting diode (LED) lighting and display technologies. The push to increase the luminous efficacy and improve the colour quality of these lights has led to a surge in reports of different combinations of phosphor host structures and activators, with many claiming that the new materials have transformative properties. This Perspective article outlines the optical property requirements phosphors must meet to impact the field. Additionally, the tools that have been developed to accelerate the discovery of exceptional phosphors that meet these requirements are summarized, including crystal-chemical design rules, proxies, data-driven approaches, first-principles calculations and combinatorial methods. We also highlight open challenges in the field of phosphor discovery. Finally, we discuss the reality that these methods are unlikely to identify a perfect phosphor that satisfies all the requirements. Instead, we propose a workflow for phosphor discovery that prioritizes the properties necessary to produce next-generation phosphor materials.

Sections

Introduction

Phosphor optical property targets

Tools for phosphor discovery

Outlook and conclusions

¹Department of Chemistry, University of Houston, Houston, TX, USA. ²Texas Center for Superconductivity, University of Houston, Houston, TX, USA. ³GE Global Research Center, Niskayuna, NY, USA. ⊠e-mail: shruti.hariyani@gmail.com; jbrgoch@uh.edu

Introduction

In 2013, the United Nations Environmental Programme estimated that lighting accounted for 20% of electricity consumption and 6% of CO₂ emission worldwide¹. The transition to phosphor-converted light-emitting diode (pc-LED) technologies has therefore drawn considerable attention for next-generation lighting owing to their small and durable form factor, high energy efficiency, long operational lifetime and environmentally benign components^{2,3}. Replacing just ~35% of conventional incandescent and discharge lights with pc-LEDs has already made a tremendous environmental and economic impact with estimated site energy (the energy consumed as reflected in utility bills) savings of 185 TWh per year, which equates to 79 million metric tonnes of CO₂ emissions being avoided and US\$20 billion saved by consumers4. If pc-LED adoption continues at its current rate, energy savings are projected to increase to ~450 TWh per year by 2035. The US Department of Energy (DOE) estimates that further advances in pc-LED technology, such as increasing device efficiency, could reduce site energy usage by a further 20% (~572 TWh per year)4.

The current generation of pc-LEDs, which are responsible for these energy savings, all operate following similar device architectures. The emission from a blue-emitting In_{1-x}Ga_xN (emission wavelength of $\lambda_{\rm em} \approx 440-460$ nm) or violet-emitting GaN ($\lambda_{\rm em} \approx 395-415$ nm) semiconducting LED chip is down-converted using inorganic phosphors to produce a broad-spectrum white light⁵. A phosphor is a luminescent solid, which is coated on or near the surface of the LED chip. The optical properties of a phosphor stem from crystal-chemical interactions between a crystalline host material, often an oxide, (oxy-)halide, (oxy-) sulfide or (oxy-)nitride, and a rare-earth or transition metal activator ion, which has been partially substituted within the host structure and acts as a luminescence centre^{3,6,7} (Fig. 1a). The rare-earth ions that are most often studied include Ce³⁺ and Eu²⁺, which undergo $4f^{n-1}5d^1 \leftrightarrow 4f^n5d^0$ Laporte-allowed electronic transitions, or Eu³⁺ and Tb³⁺, which exhibit $4f^n \leftrightarrow 4f^n$ parity-forbidden transitions. Transition metal activators such as Cr^{3+} and Mn^{4+} that undergo $3d^n \leftrightarrow 3d^n$ transitions are also widely examined⁵. The combination of the emission from the LED and phosphor blend creates the necessary spectrum for white light generation and sets the minimum bar for the colour-rendering index (CRI), correlated colour temperature (CCT) and efficacy (spectral efficiency) of a device by matching the spectral power distribution of the luminescent materials with the sensitivity of the average human eye. The CRI quantifies the colour-rendering ability or colour reproducibility of a white light source scored on a scale from 0 (no colour reproducibility) to 100 (perfect reproducibility, achieved by black body radiators). The CCT describes the hue of the white light source from warm red (low CCT) to white to bright blue (high CCT).

Modifying the optical properties of a phosphor is one of the most cost-effective ways to improve the performance of pc-LED devices. Given the ongoing push to increase pc-LED efficacy to $\geq\!250$ lm W $^{-1}$, the focus on improving device colour quality and the vast chemical space encompassing the different combinations of host structures and activators, reports of new phosphors are being published almost daily $^{4.8}$. Regrettably, a common theme among many of these reports is grandiose assertions that each new phosphor has the optimal set of properties to make the material immediately suitable for incorporation in commercial pc-LEDs. Although these reports have valuable fundamental scientific merit, most of the new materials fall short of the basic requirements necessary for device production.

In this Perspective article, we first discuss the optical properties a phosphor must possess before it can be seriously considered for

use in various applications. The influence of these optical properties on pc-LED efficiency, colour quality and reliability is emphasized. We then highlight the data-driven tools and crystal—chemical design rules developed to aid the discovery of novel phosphors with specific, desirable optical properties. The areas in which there is a critical need to develop new tools for phosphor discovery are also discussed. Finally, discovering a single phosphor with all of the required properties is not trivial. We conclude with our viewpoint on a technical workflow that can be leveraged to develop state-of-the-art phosphors for next-generation solid-state lighting. We hope this work will provide a more realistic view of the potential of different materials for pc-LED lighting and that it can be used to accelerate the discovery of new phosphors with transformative potential.

Phosphor optical property targets

The US DOE regularly publishes a road map outlining methods and research areas to improve the efficiency, colour quality and operational lifetime (longevity) of pc-LEDs. Historically, the goal has been to achieve the most energy-efficient white light possible, colour quality notwithstanding. Therefore, the first LED light bulbs contained In_{1-x}Ga_xN LED chips that were coated with yellow-emitting Ce³⁺-substituted Y₃Al₅O₁₂ (ref. 3) (Fig. 1a). These devices produced a functional white light, but the low CRI (Ra = 70) and high CCT (>5,000 K) hindered their adoption in domestic lighting⁹. Adding a second, red-emitting phosphor such as $Sr_2Si_5N_8$: Eu^{2+} or $CaAlSiN_3$: Eu^{2+} to these devices improved the colour quality to meet the minimum standards (CRI Ra = 80 and 2,700 K < CCT < 5,000 K) for general white lighting⁹. Now, research is focused on reaching efficacies of 250 lm W⁻¹, which requires electrical-to-optical power conversion efficiencies of 60% and a spectral power distribution that is optimized with respect to the sensitivity of the human eye. The US DOE reports also discuss the current state of the commercialized phosphors being used to meet these targets, highlight areas where improvements are required and emphasize the need for new and improved luminescent materials to achieve these goals.

The US DOE reports stress the six quantifiable properties that any potential phosphor must possess to be considered for commercial applications (Fig. 1). Each feature has specific metrics that should be used to evaluate the applicability of the phosphor; additional metrics were established by a survey in 2022 of state-of-the-art phosphors⁴. Only by meeting the required values of these metrics and surpassing the properties of current state-of-the-art phosphors can it be claimed that a material has the potential to replace existing phosphors and make a meaningful impact on high-brightness general illumination LED packages.

First, for a phosphor to be considered for general illumination applications, it is imperative that it can strongly absorb LED radiation. Phosphors should have an excitation band centred near 440–460 nm (corresponding to a blue LED), or for specialized lighting applications, 395–415 nm (corresponding to a violet LED). However, this property alone is not sufficient for a phosphor to be adopted for commercial applications. Phosphors should also have an absorption coefficient of >50 cm $^{-1}$ with particle sizes $(d_{50}) > 5 \, \mu \mathrm{m}$ in these excitation ranges (Fig. 1b). This first criterion precludes all phosphors that only absorb ultraviolet light $(\lambda_{\mathrm{abs}} < 380 \, \mathrm{nm})$ and phosphors with absorption bands stemming from $4f^n \leftrightarrow 4f^n$ transitions (such as Eu $^{3+}$ -substituted, Tb $^{3+}$ -substituted or Sm $^{3+}$ -substituted materials) from serious consideration for general illumination applications.

The second requirement specified by the US DOE is for highefficiency photoluminescence from red-emitting, green-emitting and blue-emitting phosphors, which is quantified by the photoluminescent

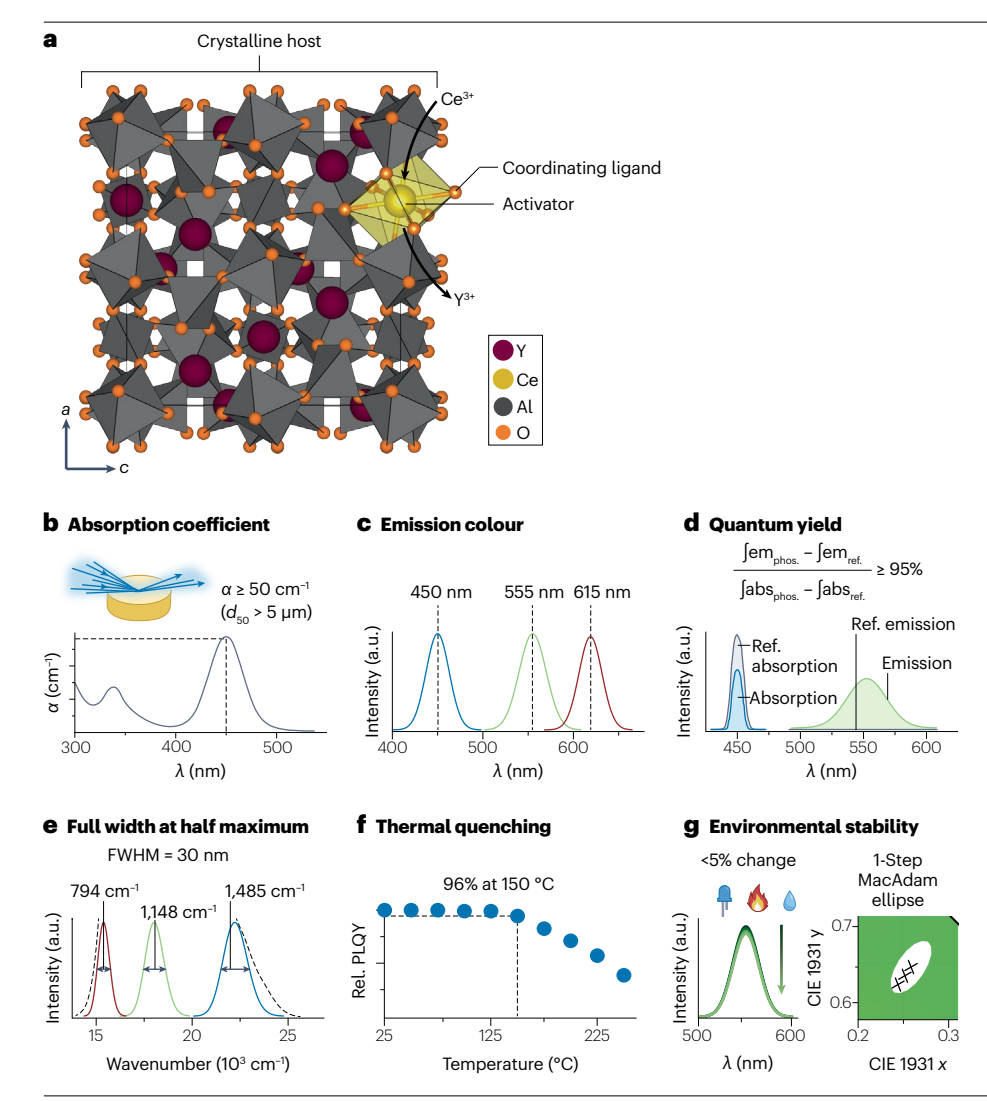


Fig. 1 | The composition of phosphors and the six key properties a phosphor must possess for commercialization. a, Phosphors comprise a crystalline host structure that has been substituted with a small percentage of an activator ion. An example host crystal structure is Y₃Al₅O₁₂, which contains oxygen atoms coordinating Y3+ and A13+ cations, that is substituted with Ce3+. b-g, Six key properties of a phosphor. Phosphors should have an absorption coefficient $\alpha \ge 50 \text{ cm}^{-1}$ (with an average particle size, $d_{50} > 5 \mu m$) across light-emitting diode wavelengths (λ) of interest (part **b**); produce a desirable emission colour with a peak emission at $\lambda_{\rm em,max} \approx 450 \text{ nm}, \lambda_{\rm em,max} \approx 555 \text{ nm and } \lambda_{\rm em,max} \approx 615 \text{ nm},$ for blue, green and red light, respectively (part c); have a photoluminescent quantum yield (PLQY) ≥95%, which can be quantified by the integrated ratio between the photons emitted (green, emphos) and the photons absorbed (blue, abs_{phos}) by the phosphor relative to a reference (grey) (part d); have a full width at half maximum (FWHM) of 30 nm, which corresponds to FWHM = 1,485 cm⁻¹, $FWHM = 1,148 \text{ cm}^{-1} \text{ and } FWHM = 794 \text{ cm}^{-1} \text{ for }$ blue-emitting, green-emitting and red-emitting phosphors, respectively, that falls within the photopic curve of a human (dashed, grey line) (part e); resist thermal quenching by retaining ≥96% of the room temperature PLQY at 150 °C (part f); and exhibit <5% change in their optical properties with the emission colour remaining within a 1-step MacAdam ellipse upon exposure to non-ambient conditions such as high-intensity incident light flux, elevated temperatures and high relative humidity (part g). The MacAdam ellipses are plotted on the CIE (Commission Internationale de l'Eclairage, or International Commission for Illumination) 1931 colour space. a.u., arbitrary unit.

quantum yield (PLQY). The need for red-emitting and green-emitting materials with emission bands (λ_{em}) around \approx 615 nm and \approx 555 nm, respectively, arises from the goal of simultaneously maximizing pc-LED efficacy and colour rendering (Fig. 1c). The target of the US DOE is to produce new green-emitting and red-emitting phosphors with a PLQY of 99% and 95%, respectively (Fig. 1d). Research into blue-emitting phosphors with emission bands centred at $\lambda_{em} \approx 450$ nm has been reinvigorated owing to their potential application for human-centric lighting⁴. Human-centric lighting aims to minimize exposure to harmful blue light by using a violet LED and trichromatic (red-emitting, green-emitting and blue-emitting) phosphor mixture in which the emission intensity of the blue-emitting phosphor can be intentionally minimized. However, the blue-emitting phosphors must absorb radiation from a violet LED to be of potential interest, eliminating the majority of blue-emitting phosphors that only absorb shorter ultraviolet wavelengths¹⁰. If a desirable excitation spectrum is achieved in a blue-emitting phosphor, it should also possess a PLQY of 99%. The main bottleneck in the commercialization of blue-emitting phosphors is that it is rare for a phosphor to have a small enough Stokes' shift to be able to absorb and down-convert violet light into blue light and even rarer to perform this process efficiently. Therefore, BaMgAl₁₀O₁₇:Eu²⁺ (PLQY = 90%, $\lambda_{\rm ex}$ = 400 nm) is, to the best of our knowledge, the only commercialized blue-emitting phosphor¹⁰.

The full width at half maximum (FWHM) and maximum position $(\lambda_{em \, max})$ of the phosphor emission dictate the spectral coverage of LED packages for general lighting, the colour gamut of displays and the energy efficiency of each device9. For example, red-emitting nitride and oxynitride phosphors typically have an FWHM of ~100 nm (~2,100 cm⁻¹). This broad FWHM causes the emission spectrum to extend into the near-infrared region, where the human eye is less sensitive¹¹. The photons emitted in wavelength regions beyond the sensitivity of the human eye are lost because they are not perceived, which lowers the efficacy of current LED packages. Therefore, the US DOE has set a long-term target that phosphors used in pc-LEDs should have an FWHM of 30 nm across the visible spectrum (Fig. 1e). Using narrow band red-emitting phosphors can reduce spillover emission into the near-infrared and has been reported to increase device efficacy by $22\%^{4,11}$. However, it is essential to note that achieving FWHM = 30 nmis not only a difficult task for inorganic phosphors, but using only three (red, blue and green) narrow emission bands in devices will yield

lower colour rendering capabilities¹². This limitation is exemplified by a model white light spectrum created from a trichromatic, all LED architecture. Using a red-emitting ($\lambda_{em.max}$ = 605 nm), green-emitting $(\lambda_{\rm em,max}$ = 540 nm) and blue-emitting $(\lambda_{\rm em,max}$ = 455 nm) LED, each with an FWHM of 5-10 nm, is expected to achieve 408 lm W⁻¹ but provides a CRI Ra score of only 80 (ref. 13). CRI Ra = 80 is the minimum score that is acceptable for general illumination; therefore, this result emphasizes the limitation of building lighting devices that maximize efficacy at any cost¹⁴. Thus, current research endeavours are focused on identifying an appropriate LED and phosphor blend that minimizes the gap between energy efficiency and colour quality to produce a highly efficient LED package with a CRI Ra = 90. In most cases, novel phosphors should be evaluated by creating phosphor blends using relevant industry phosphors as baselines. For example, the potential impact of a new green-emitting phosphor on pc-LED colour quality can be assessed by creating a white light spectrum using a blue LED and a commercial red-emitting phosphor and comparing the optical properties of the prototype with those of commercial pc-LEDs.

A phosphor should also be thermally and chemically robust to ensure the longevity of pc-LEDs. The LED chip in these devices generates heat, reaching temperatures up to 150 °C (423 K) during operation. As a result, it is imperative that the emission intensity of the phosphor is retained even at these elevated temperatures. The US DOE recommends that phosphors maintain 96% of their room temperature emission intensity at 150 °C as even minor losses in photoluminescence contribute to losses in efficiency (Fig. 1f). To achieve device longevity, a phosphor should be robust with respect to external stimuli, meaning that it must retain its average crystal structure and optical properties upon exposure to the high-intensity incident light flux, elevated temperatures and ambient moisture encountered throughout the operational lifetime of a device (Fig. 1g). Relative changes in phosphor efficiency over time can lead to both efficacy losses and shifts in the perceived colour of the device as the balance of LED and phosphor emission that makes up the white light can be altered. The chromatic stability of a phosphor or general white light source with respect to these applied stimuli can be quantified by calculating $\Delta u' \Delta v'$, which is defined as the distance between the ambient (initial) colour point and the average colour point as a function of the applied stimulus (for example, temperature, humidity and incident light). This $\Delta u' \Delta v'$ distance and all of the stimuli-dependent colour coordinates should fall within a 1-step MacAdam ellipse for a phosphor or a 4-step MacAdam ellipse for a white light source centred on the initial chromaticity coordinate to minimize perceptible shifts in colour¹⁵.

Tools for phosphor discovery

Identifying new, competitive phosphors that meet all the requirements of the US DOE (Fig. 1) using traditional methods, such as systematic materials synthesis, is non-trivial. Indeed, as the field expands, this historically lucrative research area is becoming more concentrated, challenging and expensive, decreasing the likelihood that superior phosphors can be identified. Therefore, substantial efforts have gone into establishing crystal—chemical design rules and building high-throughput and data-driven tools to increase the probability of discovering new phosphors with exceptional optical properties. These efforts are largely focused on the characteristics outlined subsequently.

Emission colour of $4f \leftrightarrow 5d$ transitions

It is generally understood that the $4f^n \rightarrow 4f^{n-1}5d^1$ absorption and $4f^{n-1}5d^1 \rightarrow 4f^n$ emission of Ce^{3+} -substituted and Eu^{2+} -substituted phosphors stems

from a combination of crystal field splitting and the nephelauxetic effect (centroid shift) (Fig. 2a). This leads to a redshift of the excited 5d energy levels when compared with energy levels of lanthanide ion as a free ion in a vacuum. The redshift describes the phenomenon of the energy of the rare-earth 5d orbitals decreasing upon substitution in a host crystal structure. Its magnitude depends on the distance between the rare-earth or transition metal activator ion and its coordinating ligands and the coordination, symmetry and charge of the activator site. Specific symmetry environments that induce strong crystal field splitting, such as dodecahedral, octahedral and cubic substitution sites, are sought to produce red-shifted $4f^{n-1}5d^1$ energy levels¹⁶. Similarly, the activator-ligand bond length is often manipulated by creating solid solutions, which enables a tunable $\lambda_{\rm em,max}$. For example, substituting Ca²⁺ and [PO₄]³⁻ pairs for La³⁺ and [SiO₄]⁴⁻ following $Ca_{2+x}La_{8-x}(SiO_4)_{6-x}(PO_4)_xO_2$: Eu²⁺ influences the magnitude of crystal field splitting and degree of covalency, shifting the blue emission $(\lambda_{\rm em.max} = 460 \text{ nm})$ of the parent phosphor to the green region of the visible spectrum¹⁷ ($\lambda_{\text{em,max}} = 508 \text{ nm}$). Finally, the covalency of the ligand can be used to target different regions of the visible spectrum. Halides tend to be relatively ionic, meaning that they do not induce a strong nephelauxetic effect and tend to undergo weak crystal field splitting. These phosphors typically produce blue-shifted absorption and emission bands. Oxides, and to a greater extent, nitrides, tend to be relatively covalent and undergo stronger crystal field splitting than halides, leading to the generation of blue, green or red emission bands³ (Fig. 2a).

These crystal–chemical handles can be used as a screening tool to increase the probability of obtaining a particular emission colour or to tune the emission from a known phosphor. However, they cannot guarantee a specific emission colour. There has been some success in using machine learning and other data-driven techniques to predict $\lambda_{\rm em,max}$, but these models are usually limited to specific systems (such as garnets) or stoichiometries ^{18,19} (such as $A_3BSi_2O_7$). The van Uitert equation, which was derived from empirical relationships to predict $\lambda_{\rm em,max}$, is more universal and can be applied to any Eu²⁺-substituted or Ce³⁺-substituted phosphor

$$\lambda_{\text{em,max}}(\text{cm}^{-1}) = Q \left[1 - \left(\frac{V}{4} \right)^{\frac{1}{V}} 10^{-nE_{a}r/80} \right],$$
 (1)

where Q is 34,000 cm⁻¹ or 50,000 cm⁻¹, which is the position of the lower d-band edge of a free Eu²⁺ or Ce³⁺ ion, respectively, V is the valency of the activator, n is the number of coordinating anions around the activator, E_a is the electron affinity of the coordinating anions and r is the radius of the host cation replaced by the activator²⁰.

Methods that are typically used in the social sciences such as a confirmatory factor analysis 21 have also been applied to uncover any correlations between typical crystal—chemical handles and how they guide the location of $\lambda_{\rm em,max}$. Confirmatory factor analysis differs from traditional machine learning methods as it does not rely on statistical regression. Instead, it is a statistical approach that uses a set of latent variables to identify the underlying relationship between the measured variables. In one example, a carefully tailored training set of 75 Eu $^{2+}$ -substituted phosphors was used to identify four latent factors that influence $\lambda_{\rm em,max}$: the A-X local environment factor; the A-A local environment factor; the anion trait factor and the networking element trait factor, in which A and X are the Eu $^{2+}$ -substitution site and its coordinating ligand, respectively 21 . These latent factors were instrumental in understanding the differences in the emission wavelength of two

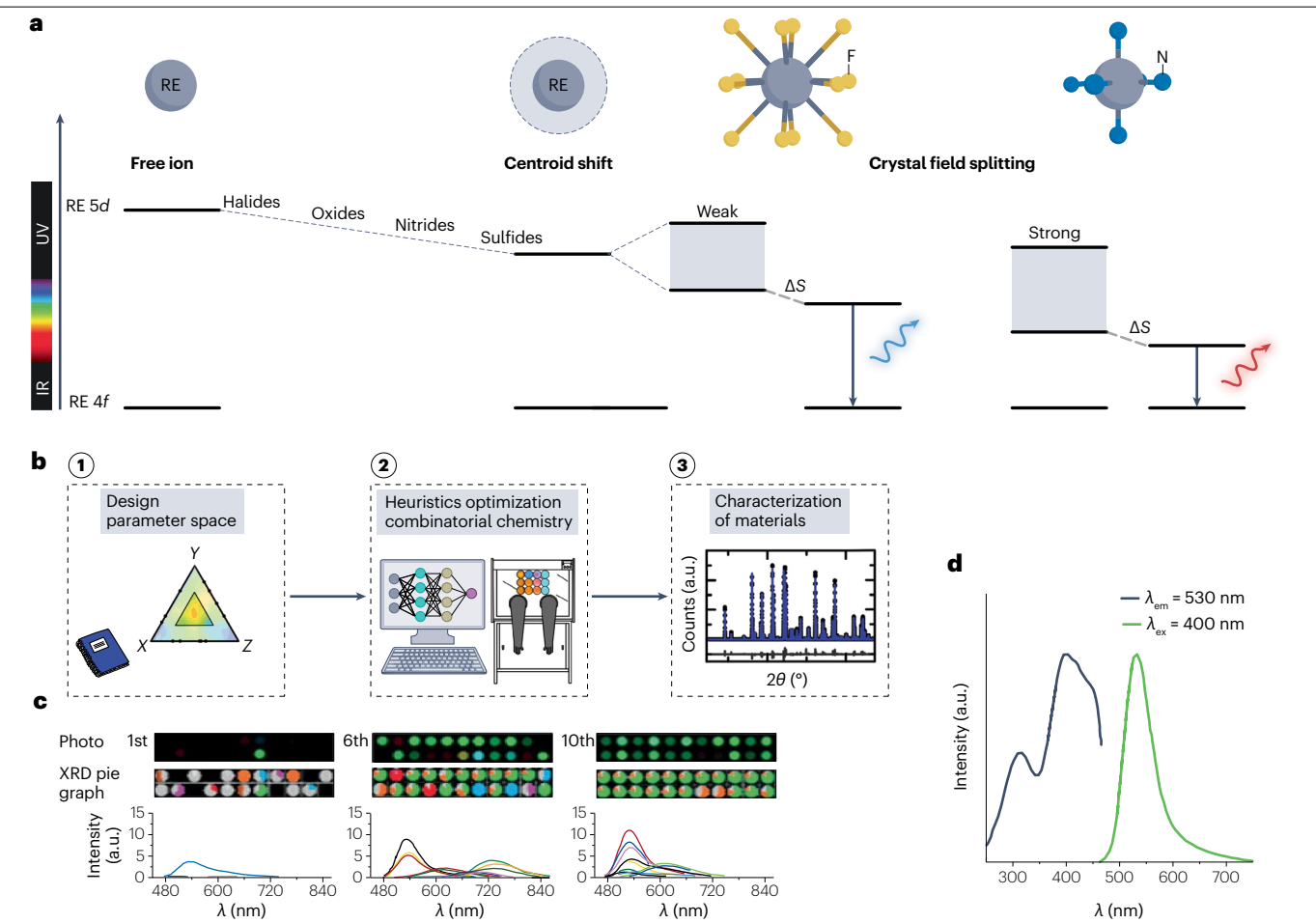


Fig. 2 | Metaheuristics-assisted combinatorial screening to target phosphors with a specific emission colour. a, The emission colour of a phosphor depends on the magnitude of the centroid shift (nephelauxetic effect) and the energy of the crystal field splitting. Free (gaseous) rare-earth (RE) ions produce deep ultraviolet (UV) luminescence. Substituting the RE ion into a host structure causes the energy of the RE 5d orbitals to decrease – an effect known as the centroid shift. Sulfides often produce a larger centroid shift than nitrides and oxides, with halides producing the smallest centroid shift. The degeneracy of the RE 5d orbitals is lifted by crystal field splitting. Radiative relaxation occurs from the lowest energy excited 5d orbital to the 4f ground state; the energy difference between these orbitals is known as the Stokes shift (ΔS). Weak crystal field splitting, which is typically observed in cuboctahedral symmetry with halide ligands (such as F⁻), produces blue-shifted emission bands. An activator octahedrally coordinated with N³⁻ undergoes strong crystal field splitting, producing red-shifted emission bands. **b**, A simplified workflow for a combinatorial approach involving heuristics optimization and high-throughput experimentation. (1) A large compositional space is selected on the basis of the current trends in literature, industry demands and chemical intuition. (2) A genetic algorithm screens this compositional

space for materials that meet the input target objective functions. The materials that the model converges upon are chosen for high-throughput synthesis. The results are then used to generate a new population for investigation. This process is iterated until the algorithm identifies a single-phase product. (3) The structure and composition of the converged phase are identified, and the optical properties are characterized with techniques such as powder X-ray diffraction (XRD). c, A data library visualization of the 1st, 6th and 10th generation of the metaheuristics-assisted combinatorial screening of the Eu²⁺-substituted Ca-Sr-Ba-Li-Mg-Al-Si-Ge-N compositional space. A photo of each of the 22 phosphor samples synthesized (top), a pie graph representing the phase fraction for each sample (middle) determined using powder XRD and the emission spectrum of each sample (bottom) are provided for each generation. d, The BaLi₂Al₂Si₂N₆:Eu²⁺ phosphor identified by the workflow in parts ${\bf b}$ and ${\bf c}$ produces the desired green emission (centred at $\lambda_{\rm em}$ = 530 nm) upon $\lambda_{\rm ex}$ = 400 nm excitation. The excitation spectrum is shown in black and the emission spectrum is shown in green. a.u., arbitrary unit; IR, infrared. Part **b** adapted with permission from ref. 103, Elsevier. Parts c and d adapted with permission from ref. 24, Copyright 2015 American Chemical Society.

structurally similar phosphors: Ba₂LiB₅O₁₀:Eu²⁺ ($\lambda_{em,max}$ = 587 nm) and BaB₈O₁₃:Eu²⁺ ($\lambda_{em,max}$ = 408 nm)^{22,23}. Although conventional crystal field theory cannot explain the differences in the photoluminescence of these two phosphors owing to their nearly identical substitution sites, the latent factors revealed that it is likely that the red-shifted emission observed from Ba₂LiB₅O₁₀:Eu²⁺ was induced by the smaller *A*–*A* distance

and A-site coordination number relative to BaB_8O_{13} : Eu^{2^+} . It is clear that many approaches to estimate or explain the emission colour of phosphors based on the position of the band centre have been tested. However, none of these approaches accounts for the FWHM or shape of the emission band, which also contributes to the observed emission colour. Moreover, the precision of these methods is relatively low.

In the absence of strong phenomenological predictors, high-throughput experimental methodologies have been developed that screen phosphors by observing the exact emission colour after synthesis. One such scheme combines heuristics optimization with high-throughput experimentation to identify novel phosphors^{24,25} (Fig. 2b). This workflow applies an elitism-reinforced nondominated sorting genetic algorithm to screen large compositional spaces of interest on the basis of the selected target objective functions. The compositions identified by the algorithm are selected for high-throughput synthesis, and the most promising are then modified by crossover and mutation methods to generate a new population. This process is iterated until the specified convergence criteria are met. The main advantage of this approach is the ability to define specific target objective functions. In one example, $\lambda_{\rm em,max}$ and the emission peak area were used as target functions to target narrow, green-emitting (λ_{em} = 530 nm) phosphors from the Ca-Sr-Ba-Li-Mg-Al-Si-Ge-N compositional space²⁴. This process required 10 generations to be iterated by nondominated sorting genetic algorithm-II with 22 phosphor samples of different compositions in each generation. With each iteration, the model got closer to the target optical properties (Fig. 2c). Indeed, the first generation included many mixed-phase samples that exhibited no luminescence, whereas later generations had improved green luminescence and phase purity. The final phase that was converged upon was BaLi₂Al₂Si₂N₆:Eu²⁺. This phosphor met the targets of the algorithm by producing a green emission band centred at 530 nm with an FWHM of \approx 2,126 cm⁻¹ (59 nm) (Fig. 2d). Although this phosphor was already known, it is clear that this method can screen vast compositional spaces to yield phosphors with targeted optical properties²⁶. Similar methods have since revealed three potential phosphors for general illumination applications: Ba(Si,Al)₅(O,N)₈:Eu²⁺ ($\lambda_{em,max}$ = 475 nm; FWHM \approx 3,280 cm⁻¹, \approx 71 nm)²⁵, Ca_{1.5}Ba_{0.5}Si₅N₆O₃:Eu²⁺ ($\lambda_{em,max}$ = 585 nm; FWHM \approx 3,264 cm⁻¹, \approx 76 nm)²⁷ and La_{4-x}Ca_xSi₁₂O_{3+x}N_{18-x}:Eu²⁺ (x = 1.456; $\lambda_{em,max}$ = 565 nm; FWHM \approx 2,264 cm⁻¹, \approx 73 nm)²⁸, and two red line-emitting phosphors for display backlighting: Mg₁₄Ge₅O₂₄:Mn⁴⁺ ($\lambda_{em,max}$ = 662 nm) and Li₃RbGe₈O₁₈:Mn⁴⁺ ($\lambda_{em,max}$ = 667 nm)^{29,30}. In each case, the new, phosphors that were identified generated a desirable emission colour, which justified further investigations.

A second phosphor discovery method known as single-particle diagnosis³¹ has also been proposed, which consists of five steps (Fig. 3a). First, a 'powder library' is created by synthesizing >50 Ce³⁺-substituted and Eu²⁺-substituted phosphors of differing stoichiometries within a chosen compositional space. Large particles from each polycrystalline product that exhibit desirable photoluminescence are then selected from the bulk using an optical microscope. The basic structural information of the particle is determined using single-crystal X-ray diffraction and the resulting lattice parameters and compositional information are indexed against crystal structure databases. Compounds that cannot be matched to these databases are

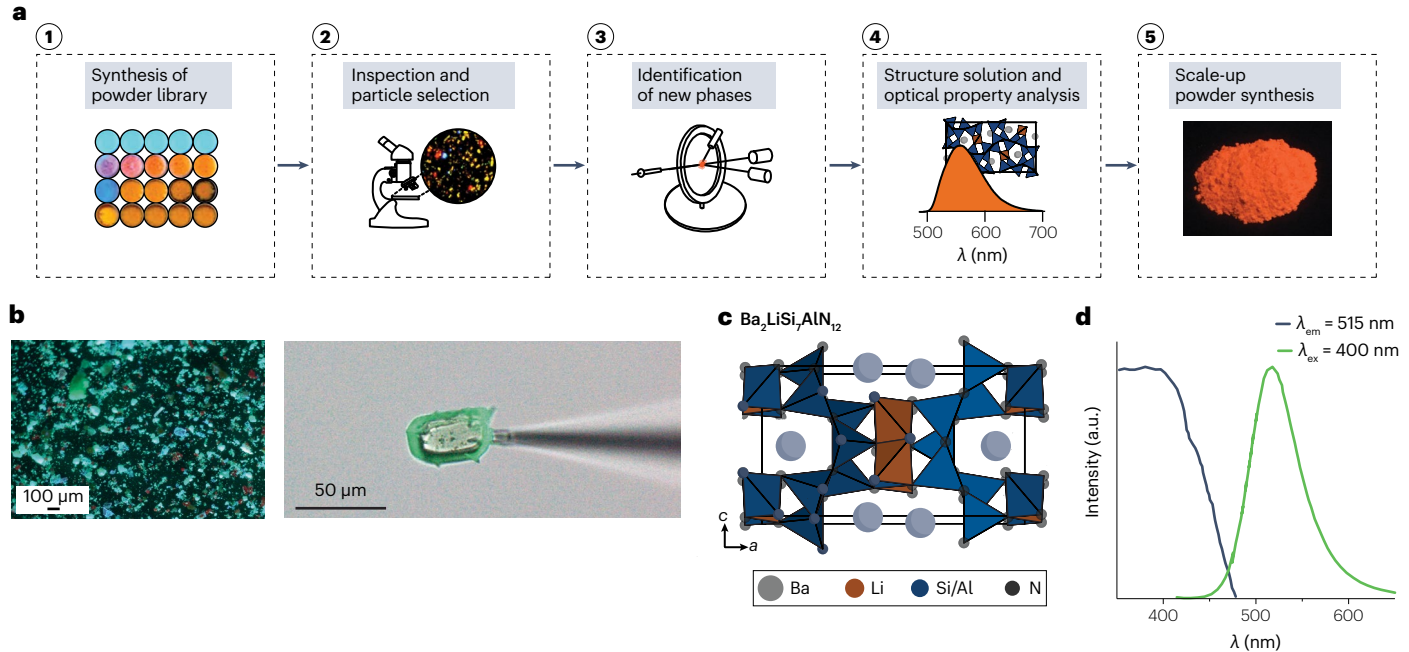


Fig. 3 | A single-particle diagnosis approach for phosphor discovery. a, The workflow for the single-particle diagnosis approach, which typically consists of five steps. (1) A 'powder library' from a chosen compositional space is formed by synthesizing over 50 compositions substituted with rare-earth ions. (2) The powder libraries are inspected for particles that exhibit the desired emission properties using a single-particle fluorescence spectrophotometer and a sufficiently large particle size under an optical microscope. (3) The structure of the chosen particle is examined using single-crystal X-ray diffraction and the solution is indexed against known phases in inorganic crystal structure databases. (4) Single-crystal X-ray diffraction is performed on systems that cannot be indexed. Additionally, full optical characterization is conducted. (5) The appropriate synthetic route to obtain a scaled-up,

phase-pure polycrystalline sample of the phosphor is investigated. **b**, Left, photograph of a powder library from step 1 under ultraviolet excitation from the 0.8Ba:0.20Eu:0.58Si:6.42Al:3Li compositional space. Right, photograph of the green-emitting particle selected in step 2 under ultraviolet excitation. **c**, Ba₂LiSi₇AlN₁₂ crystallizes with a *Pnnm* structure and is composed of corner-connecting [(Si/Al)N₄] tetrahedra that edge share with [LiN₄] tetrahedra (step 4). **d**, The identified Ba₂LiSi₇AlN₁₂:Eu²⁺ phosphor produces a green emission centred at 515 nm upon 400 nm excitation. The excitation spectrum is shown in black and the emission spectrum is shown in green. a.u., arbitrary unit. Part **a** adapted with permission from ref. 103, Elsevier, and ref. 33, Copyright 2014 American Chemical Society. Parts **b** and **d** adapted with permission from ref. 34, Copyright 2017 American Chemical Society.

treated as novel. Next, the single particle is characterized, including determining the complete crystal structure and stoichiometry and the remaining optical properties of the material (such as PLQY and thermal stability) are evaluated. Finally, an appropriate synthetic route to obtain a phase-pure bulk sample is explored.

This methodology has identified new phosphors within the oxynitridosilicate³², nitridoaluminate³³, nitridolithoaluminate³⁴ and oxonitridoalumosilicate³⁵ compositional spaces. For example, single-particle diagnosis was used to identify green-emitting Ba₂LiSi₇AlN₁₂:Eu²⁺ (ref. 34). In this case, phosphors of variable composition were synthesized within the Ba₃N₂-Li₃N-Si₃N₄-AlN phase space. The product contained a mixture of blue-emitting BaSi₇N₁₀:Eu²⁺, red-emitting Ba₂Si₅N₈:Eu²⁺, blue-emitting BaSi₆N₈:Eu²⁺ and unindexed green-emitting crystals (Fig. 3b). The structure and stoichiometry of the green-emitting product were determined to be Ba₂LiSi₇AlN₁₂:Eu²⁺, which crystallizes in the orthorhombic *Pnnm* space group (Fig. 3c). This phosphor produces a bright green emission with an FWHM of 2,280 cm⁻¹ (61 nm) and a PLQY of 79% (λ_{ex} = 400 nm) (Fig. 3d). Ultimately, single-particle diagnosis and combinatorial methods are promising for identifying novel phosphors with a specific emission colour. However, these techniques are still relatively time-consuming, synthesis-led endeavours. Therefore, there is still a critical need to understand the characteristics that control emission colour.

Photoluminescent quantum yield

One of the most important optical properties of a phosphor is the ability to efficiently absorb and down-convert photons to longer wavelengths. The efficiency of this process is often quantified by measuring the absolute PLQY³⁶. The PLQY is a general term used for two different metrics: internal quantum efficiency (IQE) and external quantum efficiency (EQE). The IQE is the integrated ratio between the photons absorbed and emitted by the luminescent centre relative to a reference, usually a blank with a known or assumed reflectance. The PLQY reported in the literature is most commonly implied to be the IQE, which is also the case in this Perspective article. Conversely, EOE describes the ratio of photons emitted versus the total incident photons and incorporates all the processes involved with photon extraction, from the absorption of incident photons (including reabsorption and energy transfer processes) to the out-coupling of photons emitted by the bulk material³⁷. It is important to note that the EQE of a material is affected by sample-dependent factors such as particle size and morphology^{38,39}. Therefore, if a material has a high IQE, synthetic and post-processing conditions can be optimized to maximize photon extraction and to increase the EQE.

The IQE and EQE of a phosphor are heavily influenced by the concentration of the activator substituted within the host. Increasing the activator concentration typically increases the PLQY of a phosphor owing to the increased absorption of incident excitation energy. However, continually increasing the activator concentration will eventually cause the PLQY to decrease owing to an increased probability of energy transfer between the activators, which results in non-radiative relaxation⁴⁰. The optimal activator concentration is one that yields the highest PLQY by maximizing the improvements in absorptivity while preventing any loss in efficiency owing to energy transfer. Therefore, new phosphors should be synthesized with various activator concentrations, typically in a range from 0.5% to 7.5%, to identify the concentration that yields the highest PLQY under a constant excitation wavelength. It is important to note that emission intensity cannot be used in lieu of PLQY measurements because an accurate quantitative comparison cannot be made owing to the arbitrary units of intensity⁴¹.

Directly predicting the IQE or EQE of a phosphor is not straightforward because there are many factors that influence the conversion efficiency. Fortunately, a series of structural design rules for achieving a high IQE have been compiled through a literature analysis of highly efficient phosphors⁴². First, the crystalline host structure must have a wide band gap $(E_a > 4 \text{ eV})$ to minimize thermally induced photoionization, which is a non-radiative pathway that decreases the IQE⁴². A second design rule to prevent non-radiative relaxation through vibration is to ensure that the host crystal structure is rigid. Structural rigidity can be investigated by examining the polyhedral networks and cationic backbone of inorganic solids. Y₃Al₅O₁₂ (Fig. 4a, left) is the prototypical example of a rigid crystal structure because it contains a network of corner-connected [AlO₄] and [AlO₆] polyhedra and a double gyroid formed from interpenetrating networks of Y and Al (ref. 43). Comparatively, BaSiO₃ (Fig. 4a, right) is unlikely to be as structurally rigid as Y₃Al₅O₁₂; this metasilicate contains isolated corner-connecting [SiO₄] tetrahedra and the cation network contains dimers of Si atoms lying in the centre of hexagonal sheets of Ba atoms⁴⁴. These isolated bonding motifs are unlikely to contribute to preventing vibration-induced non-radiative relaxation.

The variety and complex nature of chemical bonding in solids makes it difficult to compare the rigidity of host structures⁴². Instead, the Debye temperature (Θ_D) of a host structure can be used as a proxy to quantitatively compare structural rigidity⁴⁵. Experimentally determining $\Theta_{\rm p}$ involves ultrasonic pulse-echo speed of sound measurements or measurements of the low-temperature heat capacity ${}^{46}(C_p)$. Instead, it is much quicker to estimate Θ_D of a host using density functional theory (DFT) calculations ($\Theta_{\text{D,DFT}}$) than performing these experimental measurements. Therefore, $\Theta_{D,DFT}$ can be used as a proxy for the PLQY of a phosphor and ultimately as a tool for screening inorganic crystal structure databases 45,47. There is a positive correlation between the Θ_{DDET} of typical host structure families and the PLQY of the respective phosphors when substituted with the same activator ⁴⁷ (Fig. 4b). Therefore, it is not surprising that the exceptionally rigid Y₃Al₅O₁₂ has an extremely high $\Theta_{D,DFT}$ (714 K), whereas silicates such as BaSiO₃, Ba₂SiO₄ and Ba₉YSi₂Si₆O₂₄ have a lower $\Theta_{D,DFT}$ of ~227 K, 311 K and 409 K, respectively ^{46,48,49}. Additionally, $Y_3Al_5O_{12}$: Ce^{3+} has a very high PLQY of >95% (λ_{ex} = 450 nm), compared with the poorer performance of BaSiO₃:Ce³⁺ (PLQY = 28%, λ_{ex} = 340 nm), $Ba_2SiO_4:Ce^{3+}$ (PLQY = 51%, λ_{ex} = 351 nm) and $Ba_9Y_2Si_6O_{24}:Ce^{3+}$ (PLQY = 57%, $\lambda_{\rm ex}$ = 405 nm). Other host families such as oxyfluorides (such as Sr₃AlO₄F with a $\Theta_{D,DFT}$ = 465 K) and borates (such as NaMgBO₃ with a $\Theta_{D,DFT}$ = 563 K) often have Θ_D values between those of $Y_3Al_5O_{12}$ and the silicates described earlier $^{45,50}.$ These intermediate $\theta_{\rm D}$ values are reflected in the PLQY of $Sr_3AlO_4F:Ce^{3+}$ (PLQY = 83%, λ_{ex} = 400 nm) and NaMgBO₃: Ce^{3+} $(PLQY = 93\%, \lambda_{ex} = 370 \text{ nm})^{50,51}$.

This correlation between $\theta_{\text{D,DFT}}$ and PLQY has made $\theta_{\text{D,DFT}}$ instrumental in identifying new phosphors such as $Ba_2CaB_2Si_4O_{14}$: $Ce^{3+}(\theta_{\text{D,DFT}}=495\text{ K};\text{ PLQY}=54\%,\,\lambda_{ex}=350\text{ nm})$ and $BaScO_2F$: $Eu^{2+}(\theta_{\text{D,DFT}}=517\text{ K};\text{ PLQY}=80.3\pm0.5\%,\,\lambda_{ex}=340\text{ nm})^{50,52,53}$. However, it is essential to note that there are also instances in which a host with a high $\theta_{\text{D,DFT}}$ yields a phosphor with a low efficiency, such as $Ca_7Mg(SiO_4)_4$: $Eu^{2+}(\theta_{\text{D,DFT}}=601\text{ K};\text{ PLQY}=30\%,\,\lambda_{ex}=350\text{ nm})$ or $Sr_6Sc_2Al_4O_{15}$: $Eu^{2+}(\theta_{\text{D,DFT}}=468\text{ K};\text{ PLQY}=<6.5\%,\lambda_{ex}=365\text{ nm})^{54,55}$. Despite these inconsistencies, $\theta_{\text{D,DFT}}$ is a viable approach for down-selecting and identifying promising host crystal structures for experimental analysis.

The use of $\Theta_{\rm D}$ to identify phosphors has been expanded by developing a support vector regression (SVR) machine-learning model to predict $\Theta_{\rm D}$ ($\Theta_{\rm D,SVR}$) for systems, in which $\Theta_{\rm D,DFT}$ might otherwise be computationally inaccessible, for example, large, disordered cells. Thousands of compounds can be rapidly screened by using structural

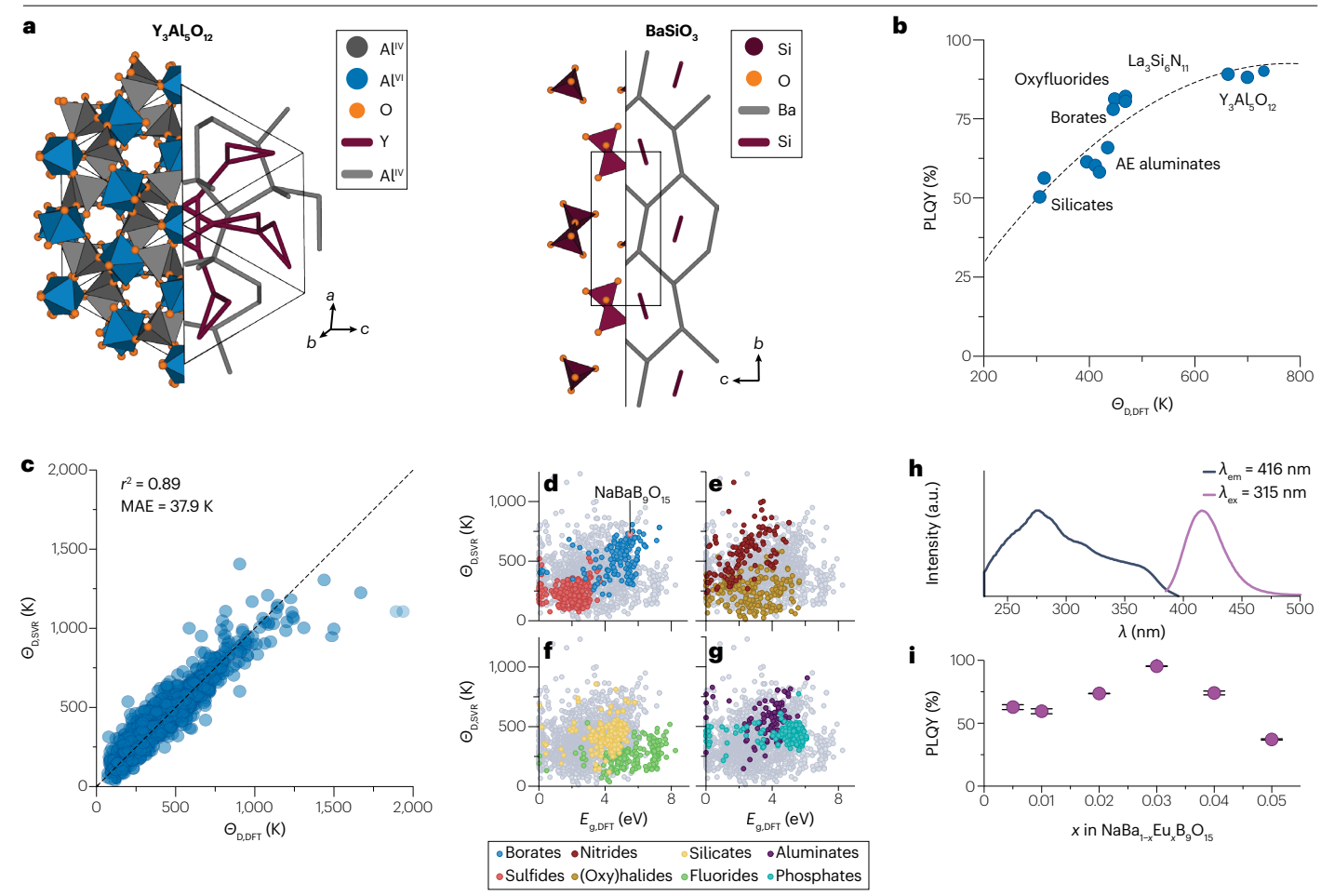


Fig. 4 | Machine learning the Debye temperature to identify highly efficient phosphors. a, Left: the crystal structure of Y₃Al₅O₁₂ (Y₃Al₂^{VI}Al₃^{IV}O₁₂) viewed from the (111) face of the unit cell. The polyhedral backbone (left) contains corner-connected [AlO₄] (grey) and [AlO₆] (blue) polyhedra, whereas the cation network (right) forms a double gyroid from the interpenetrating Y (red) and Al^{IV} (grey) atoms. The Al^{VI} atoms were excluded for clarity. Right: the polyhedral backbone of BaSiO₃ (left) contains two corner-connecting [SiO₄] tetrahedra and the cation network (right) contains dimers of Si atoms (red line) in the centre of hexagonal sheets of Ba atoms (grey). b, The measured photoluminescent quantum yield (PLQY) of phosphors is positively correlated with the Debye temperature calculated using density functional theory (DFT), $\Theta_{\text{D,DFT}}$, of common host structure families. AE aluminates are alkali earth aluminates. The dashed line is a guide to the eye. c, A cross-fold validation machine-learning model was developed to predict the Debye temperature using support vector regression (SVR), $\Theta_{\text{D,SVR}}$. The plot compares $\Theta_{D,SVR}$ with $\Theta_{D,DFT}$ for 2,071 compounds. The model has a coefficient of determination of $r^2 = 0.89$ and a mean absolute error (MAE) of 37.9 K. The ideal 1:1

line is the dashed grey line. The darker regions indicate areas of greater overlap. $\textbf{d-g}, A sorting \, \text{map generated by plotting} \, \varTheta_{\text{D,SVR}} \, \text{against the DFT-calculated band}$ gap, $E_{g,DFT}$, decomposed into the composition families, in which borate and sulfide (part d), nitride and oxy(halide) (part e), silicate and fluoride (part f) and aluminate and phosphate (part g) hosts are highlighted. Host structures that lie in the top right corner of these diagrams are predicted to have a higher probability of producing highly efficient phosphors. NaBaB₉O₁₅ (pink dot) was chosen on the basis of its high $\Theta_{\rm D,SVR}$ and $E_{\rm g,DFT}$ values. **h**, The excitation (black line) and emission (purple line) spectrum of NaBa $_{0.97}$ Eu $_{0.03}$ B $_{9}$ O $_{15}$, showing that it produces a violet $(\lambda_{\rm em,max} = 416 \text{ nm})$ emission under ultraviolet $(\lambda_{\rm ex} = 315 \text{ nm})$ excitation. i, The PLQY of $NaBaB_9O_{15}$: Eu^{2+} under 315 nm excitation as a function of Eu^{2+} concentration. The optimal Eu²⁺ concentration of 0.03 mol% yields a PLOY of 95 ± 1%. Each measurement was performed three times, with the error bars showing the standard deviation. a.u., arbitrary unit. Part a (left) adapted with permission from ref. 43. Copyright 2013 American Chemical Society, Part b adapted with permission from ref. 47, IOP. Parts c-i adapted from ref. 42, CC BY 4.0.

and compositional descriptors to accurately predict $\Theta_{D,SVR}$ (ref. 42) (Fig. 4c). Plotting $\Theta_{D,SVR}$ against the DFT-calculated band gap ($E_{g,DFT}$) of each composition creates a sorting diagram, which can be used to target host structures that are expected to yield highly efficient phosphors. The sorting diagram can be further decomposed by the composition of the host (Fig. 4d–g). Borates, such as NaBaB $_9$ O $_{15}$ (Fig. 4d, pink dot), tend to have a high $\Theta_{D,SVR}$ and wide $E_{g,DFT}$, making them suitable candidates for synthesis. Indeed, substituting 0.03 mol% of Eu²⁺

on the Ba²⁺ site in NaBaB₉O₁₅ ($\Theta_{\text{D,SVR}}$ = 729 K, $E_{\text{g,DFT}}$ = 5.5 eV) resulted in a violet-emitting phosphor (λ_{em} = 416 nm, Fig. 4h) with an excellent PLQY of 95 ± 1% (λ_{ex} = 315 nm)⁴² (Fig. 4i). Even though NaBaB₉O₁₅:Eu²⁺ produces violet emission upon ultraviolet excitation, it still possesses a sufficiently high PLQY without any post-processing, which validates the power of this machine-learning model³. Ultimately, this model can be used to rapidly identify phosphors with a high probability of meeting the efficiency requirements for pc-LEDs.

Full width at half maximum

The US DOE recommends that phosphors have an FWHM of 30 nm at all wavelengths to maximize their energy efficiency. Before discussing how to predict and tune the FWHM of a phosphor, there are some points that must be emphasized regarding how to correctly determine the FWHM. First, it is important to remember that the nanometre length scale is not linear. As a result, this wavelength-based scale incorrectly treats a FWHM of 30 nm for blue-emitting, green-emitting and red-emitting phosphors as identical⁵⁶. Instead, an energy-based scale such as the linear wavenumber scale (cm⁻¹) should be used to accurately compare the FWHM of phosphors. A 30-nm FWHM target for a blue-emitting, green-emitting and red-emitting phosphor is equivalent to FWHM \approx 1,485 cm⁻¹ ($\lambda_{em,max}$ = 450 nm), FWHM \approx 1,148 cm⁻¹ ($\lambda_{em,max}$ = 555 nm) and FWHM \approx 794 cm⁻¹ ($\lambda_{\text{em.max}}$ = 615 nm), respectively. If the $\lambda_{\text{em.max}}$ of a phosphor is not at these specific wavelengths, then the FWHM target will slightly differ. Ultimately, all FWHM data should be presented in units of wavenumbers as its value is not dependent on wavelength.

Data collected from a standard spectrophotometer are usually in units of signal per unit wavelength; therefore, the FWHM of a phosphor should only be determined once an intensity correction has been applied to convert the data to units of signal per unit energy (wavenumber) to obtain the corrected intensity in wavenumbers $I_{E_{cor}^{-1}}$.

$$I_{E_{\text{cm}^{-1}}} = I_{\lambda} \left(\frac{10^7}{(E_{\text{cm}^{-1}})^2} \right),$$
 (2)

in which I_{λ} is the intensity in nanometres and $E_{\rm cm^{-1}}$ is the energy in wavenumbers 57 . Applying this correction selectively enhances the intensity at longer wavelengths and induces a slight redshift of $\lambda_{\rm em,max}$. The effect of this transformation is most noticeable in materials that produce an emission spectrum with a broad FWHM 58 . This process is similar to the Jacobian transformation, which is applied to convert data from nanometres into energy in units of electronvolts 58 . Performing an intensity correction is critical for correctly analysing photoluminescence spectra.

The FWHM is governed by the magnitude of electron-phonon coupling and the equilibrium distance between the ground and excited state potential energy surfaces (ΔR), which approximately represents the changes in bonding that occur when an electron is excited to a higher energy level⁵⁹. Phosphors with weak electronphonon coupling, such as systems substituted with trivalent lanthanides such as Tb³⁺, Pr³⁺, Eu³⁺ or Dy³⁺ that undergo $4f^n \leftrightarrow 4f^n$ parity forbidden transitions, exhibit virtually no displacement of the excited state parabola⁵⁹. Therefore, $\Delta R = 0$, and the emission spectra of these materials are composed of sharp lines. These line emitters typically have a FWHM on the order of tens of wavenumbers (≈2–8 nm) and have some transitions located at or close to desired wavelength regions^{4,5}. The excitation spectra of these phosphors usually have two distinct features: a broad band located at ultraviolet wavelengths, which stems from charge transfer, or $4f \rightarrow 5d$ absorption, and sharp lines, which span the ultraviolet-to-visible region. Unfortunately, these phosphors cannot sufficiently cover the emission range of blue and violet LEDs without a sensitizing ion. The forbidden $4f^n \leftrightarrow 4f^n$ transitions also have weak absorption cross-sections; therefore, a large phosphor loading is required to effectively convert the LED emission. Conversely, phosphors substituted with Ce^{3+} or Eu^{2+} exhibit Laporte-allowed $4f \leftrightarrow 5d$ transitions and have a strong LED absorption. The electron-phonon coupling of these materials ranges between intermediate ($\Delta R > 0$) and strong ($\Delta R > 0$), resulting in emission bands with FWHM as narrow

as FWHM \approx 1,200 cm⁻¹ (25 nm) and as broad as FWHM \approx 7,057 cm⁻¹ (230 nm), respectively ^{59,60}.

There are no currently available methods to explicitly predict the FWHM of a phosphor. However, the FWHM can be tuned through a set of design rules that have been developed. These design rules are the best method to obtain narrow-emitting phosphors that meet the US DOE target of FWHM = 30 nm (ref. 4). The first criterion is simple – the choice of rare-earth ion. Ce³⁺ is not ideal because the activator has spin-orbit-coupled 4f ground states (${}^{2}F_{5/2}$ and ${}^{2}F_{7/2}$); therefore, relaxation to the ground state always produces two distinct emission bands. Instead, phosphors with a narrow FWHM are most often achieved in Eu²⁺-substituted phosphors⁶¹⁻⁶³. Next, a rigid host structure should be chosen to minimize diversity in radiative relaxation pathways that can lead to an inhomogeneous broadening of the emission band. Therefore, $\Theta_{D,DFT}$ could be a useful screening tool to identify phosphors with a narrow FWHM. Host structures should also contain a single crystallographically independent substitution site to ensure that only one distinct emission band is produced. Examples of such structures include $Sr_{0.99}Eu_{0.01}[Be_6ON_4]$ (FWHM = 1,400 cm⁻¹, 35 nm), $Ba_{0.99}Eu_{0.01}Li_2[Be_4O_6]$ $(FWHM = 1,200 \text{ cm}^{-1}, 25 \text{ nm}) \text{ and } NaBa_{0.97}Eu_{0.03}B_9O_{15}(FWHM = 1,962 \text{ cm}^{-1})$ 34.5 nm)^{61,62,64}. One common theme of these narrow-emitting phosphors is that the rare-earth substitution occurs on an isovalent position. Aliovalent substitution should be avoided because point defects can cause variations in the local rare-earth environment, causing the emission FWHM to broaden owing to subtle differences in crystal field splitting and the production of multiple nearly overlapping emission bands. For example, substituting Eu²⁺ on the aliovalent Na⁺ position in $NaBaB_9O_{15}$ produces the green-emitting $Na_{0.97}Eu_{0.03}BaB_9O_{15}$ phosphor, which has an FWHM (2,294 cm⁻¹, 61 nm) that is far broader than that of the violet-emitting NaBa_{0.97}Eu_{0.03}B₉O₁₅ (FWHM = 1,962 cm⁻¹, 34.5 nm)^{42,65} (Fig. 5a). In some cases, these defect states can be filled to produce an overall charge-neutral host structure by substituting an alkali or alkali earth metal such as Li⁺, Na⁺ or Mg²⁺; however, this is not always the case⁶⁶.

The requirement for a single activator substitution site can be relaxed if the local rare-earth substitution environments are nearly identical to enable an almost uniform crystal field splitting⁶⁷. An example of this can be seen in Sr[LiAl₃N₄]:Eu²⁺ (ref. 68), which crystallizes in a low symmetry, distorted derivative of the UCr₄C₄ structure type and contains two crystallographically independent [SrN₈] cuboid environments for rare-earth substitution (Fig. 5b, left). As the name suggests, both cuboid environments are slightly distorted. Most importantly, the cuboids are almost identical in volume and average bond length. The result is a narrow red emission band ($\lambda_{em.max}$ = 654 nm) with a FWHM of only 1,180 cm⁻¹ (50 nm) upon Eu²⁺ substitution⁶⁸ (Fig. 5b, left). This placement and narrow FWHM of this emission band could increase the spectral efficiency of general illumination light bulbs because few photons are emitted beyond ~14,000 cm⁻¹ (grey shaded region, Fig. 5b), which is near the perception limit of the average human eye⁹. A narrower emission band was predicted to arise in Sr[Mg₂Al₂N₄] because it crystallizes in the exact UCr₄C₄ structure with a single, perfect cubic substitution site⁶⁹ (Fig. 5b, right). Substituting Eu²⁺ produces a red emission ($\lambda_{\rm em,max}$ = 619 nm), but the FWHM was broader than anticipated (1,823 cm⁻¹, 80 nm) (Fig. 5b, right). The wide emission band was attributed to the disordered [(Mg/Al)N₄] tetrahedra, which produce variable (Al3+/Mg2+)-N bond distances. This variation influences the neighbouring edge-sharing [EuN₈] polyhedral environment and probably causes inhomogeneous broadening of the emission band⁶⁹ (Fig. 5b, right). Therefore, disordered crystal structures should also be avoided when targeting narrow emission bands.

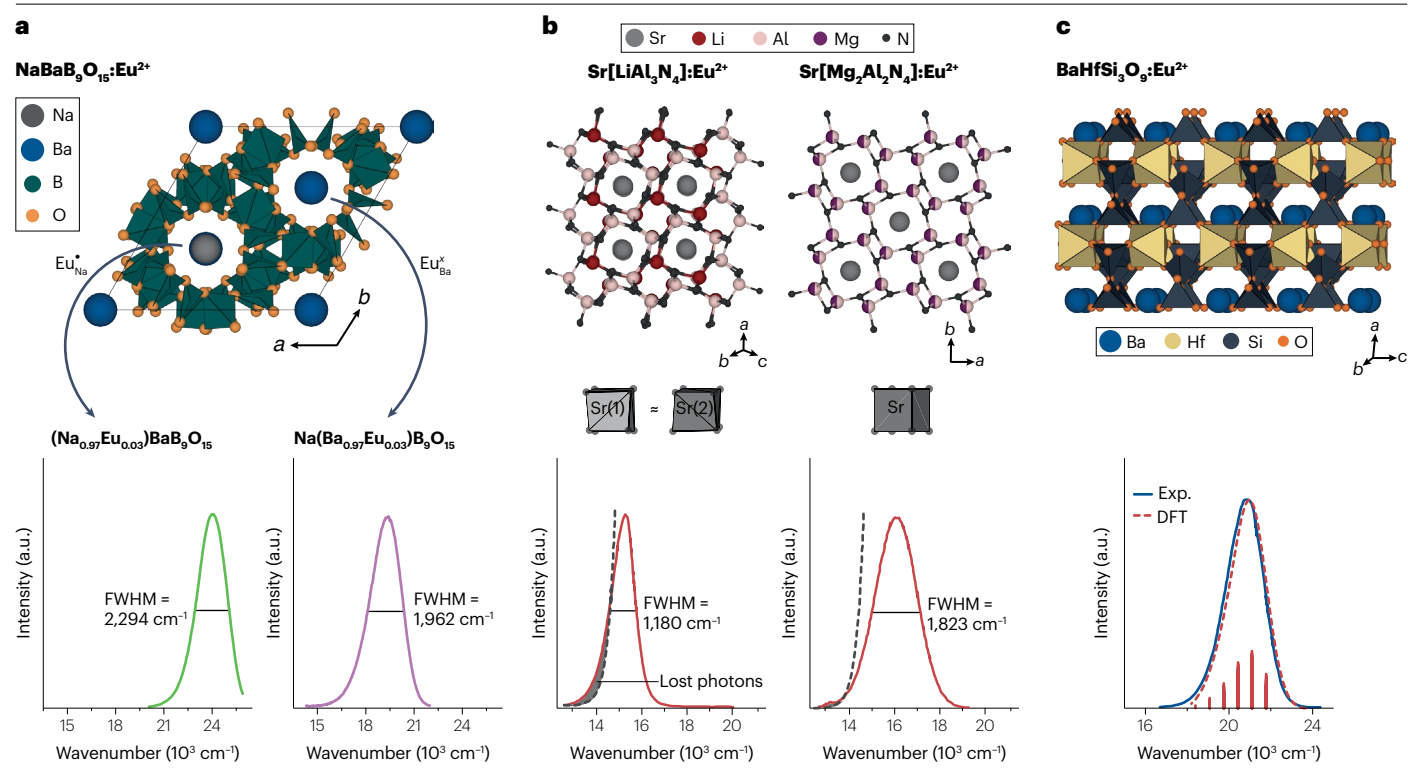


Fig. 5 | The full width at half maximum of phosphors is influenced by aliovalent substitution and local structure. a. Aliovalent substitution can lead to an inhomogeneous broadening of the full width at half maximum (FWHM) of the emission spectrum of a phosphor. Substituting Eu²⁺ for Ba²⁺ in NaBaB $_9$ O $_{15}$ (bottom right) results in a phosphor with an FWHM of 1,962 cm $^{-1}$ (34.5 nm), whereas substituting Eu²⁺ on Na⁺ (bottom left) results in a phosphor with an FWHM of 2.294 cm⁻¹ (61 nm). The substitution is indicated in Kroger-Vink notation, in which × and · refer to a neutral and positively charged point defect, respectively. **b**, Top, structures of Sr[LiAl₃N₄] (left) and Sr[Mg₂Al₂N₄] (right). Bottom left, substituting Eu²⁺ onto the Sr²⁺ site of Sr[LiAl₃N₄], which is a low symmetry derivative of the UCr₄C₄ structure type, produces a narrow red emission band with an FWHM of 1,180 cm⁻¹ (50 nm). This narrow emission band is due to the two nearly identical and highly symmetric Sr-centred cuboid substitution sites. Bottom right, substituting Eu²⁺ in Sr[Mg₂Al₂N₄], which crystallizes in the exact UCr₄C₄ structure type, results in a wider red emission band of 1,823 $cm^{\text{--}1}(80\,\text{nm})$, even though this host contains only one cubic site

for rare-earth substitution. The wide FWHM is widely attributed to the Mg-Al disorder present in the host. The dashed grey line indicates the limit of human perception and the filled light grey region indicates lost photons. c, Top, the structure of BaHfSi $_3$ O $_9$. Bottom, the FWHM of BaHfSi $_3$ O $_9$:Eu $^{2+}$ is ~2,100 cm $^{-1}$ (50 nm). The blue line is the experimentally observed emission spectrum, which agrees well with the density functional theory (DFT)-calculated FWHM of ≈2.060 cm⁻¹ (48 nm). The red lines represent the Frank-Condon factors from the lowest vibrational mode of the lowest energy 4f65d state to the different vibrational modes of the 4fst ground state. The red dashed line shows the envelope of the Frank-Condon factors calculated using DFT, which is the simulated emission curve. a.u., arbitrary unit. Part a (right) adapted from ref. 42, CC BY 4.0. Part a (left) adapted with permission from ref. 65, Copyright 2021 American Chemical Society. Part b (bottom left) adapted from ref. 68, Springer Nature Limited. Part b (bottom right) adapted with permission from ref. 69, Copyright 2014 American Chemical Society. Part c adapted with permission from ref. 70, Wiley.

Currently, the FWHM of an inorganic phosphor can only be estimated by calculating the Franck–Condon factors (F_n) using DFT. The Franck–Condon factor for the transition from the lowest energy vibrational mode of the excited state to the nth vibrational mode of the ground state is

$$F_n = \frac{e^{-S}S^n}{n!},\tag{3}$$

$$S = \frac{m\omega}{2\hbar} \, \Delta R^2,\tag{4}$$

in which S is the Huang Rhys parameter, which can be calculated with equation (4), in which m and ω are the reduced mass and oscillation frequency of the vibrating system, respectively 70,71 . Determining m and

 ω with DFT is non-trivial, but when these calculations are performed, the FWHM of BaHfSi₃O₉:Eu²⁺ (FWHM ≈ 2,100 cm⁻¹, 48 nm) shows excellent agreement with the experimental value (FWHM ≈ 2,060 cm⁻¹, 50 nm)⁷⁰ (Fig. 5c). Developing a machine-learning model to first predict S and then F_n could be one possible method to rapidly predict the FWHM of a phosphor. However, such an approach would require an extensive training data set of S values.

Thermal quenching resistance

High-power LED and laser-driven lighting solutions require that the emission intensity of a phosphor remains robust to the heat produced by these excitation sources. Thermal contact between the phosphor and LED as well as heating from Stokes losses can cause the phosphor to experience temperatures up to 150 °C (423 K). This heat can provide sufficient energy to activate non-radiative relaxation pathways that

reduce the photoluminescence intensity⁷². The thermal stability of a phosphor is often quantified by the so-called thermal quenching temperature (T_{50}), which is the temperature at which the phosphor loses 50% of its low-temperature emission intensity. The majority of phosphor publications assert that a phosphor is thermally stable if it has a $T_{50} \ge 423$ K, but this is clearly inadequate for withstanding the thermal conditions in LED packages. The US DOE recommends that phosphors should not lose more than 4% of their room temperature emission intensity at temperatures up to 423 K, meaning that

the thermal stability of phosphors should instead be assessed by measuring T_4 (ref. 4).

Nevertheless, identifying thermally robust phosphors requires understanding the thermal quenching mechanisms in phosphors. There are two dominant quenching pathways in rare-earth substituted phosphors that undergo Laporte-allowed $4f \leftrightarrow 5d$ transitions: thermally induced photoionization and excited-state crossover relaxation. Thermally induced photoionization (Fig. 6a) posits that thermal quenching is caused by the temperature-induced promotion of

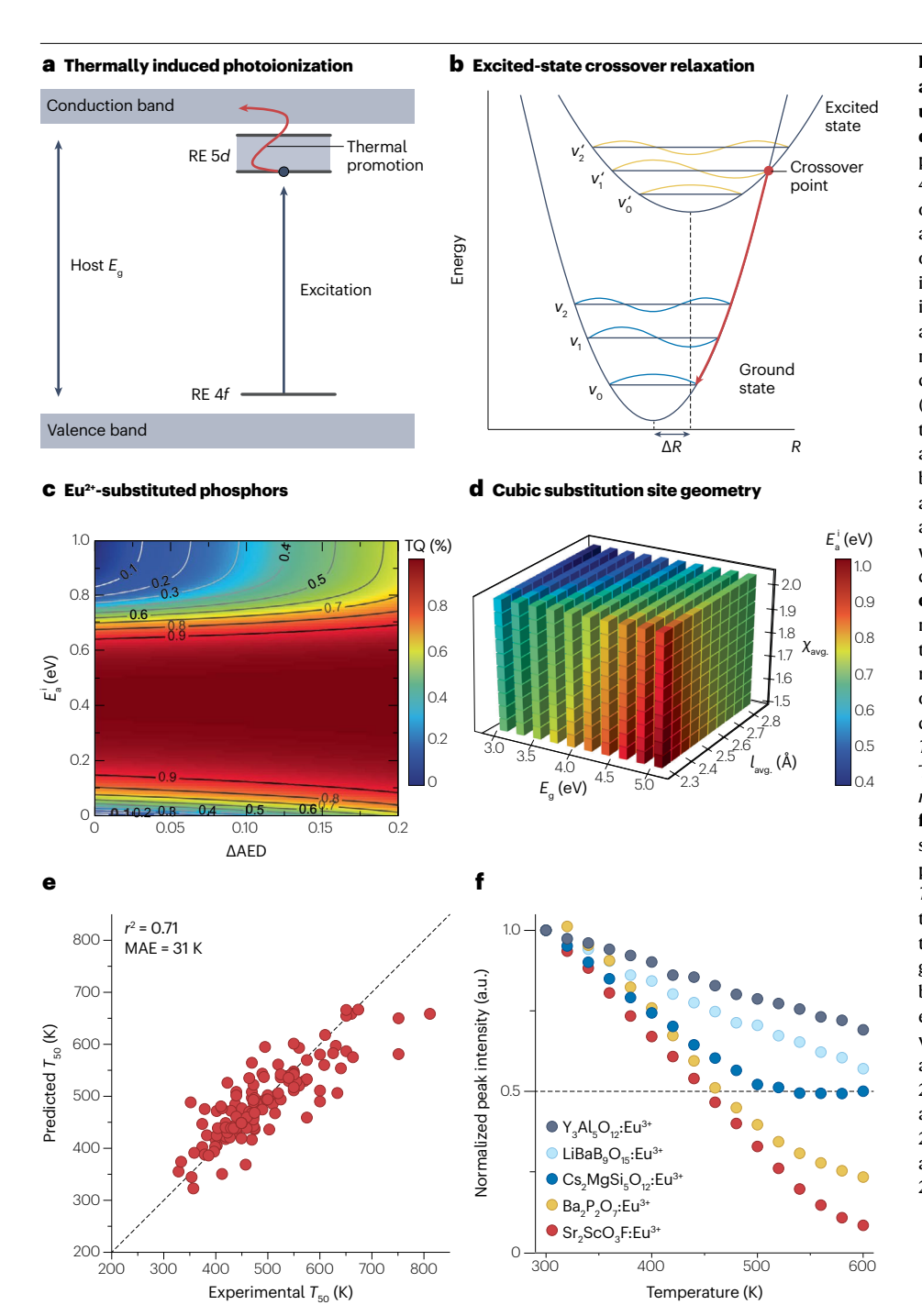


Fig. 6 | Density functional theory calculations and machine learning can be used to understand and predict phosphor thermal quenching. a, Schematic of thermally induced photoionization in phosphors that undergo $4f^{n-1}5d^1 \leftrightarrow 4f^n5d^0$ transitions. Thermal quenching occurs due to the thermally induced promotion of a photon into the conduction band. **b**, Schematic of the crossover mechanism in which thermally induced non-radiative relaxation occurs at the intersection (crossover) point between the ground and excited state parabolas. c, A phosphor design map for Eu2+-substituted phosphors. The plot depicts the predicted thermal quenching (TQ) percentage as a function of the difference in the activator environment distribution at 300 K and 500 K (Δ AED) and the thermal ionization barrier E_a^i , **d**, The predicted E_a^i as a function of E_g , average activator-ligand bond length (l_{avg}) and average cation electronegativity (χ_{avg}) for hosts with a cubic substitution geometry. These maps can be used to target thermally robust phosphors. e, A support vector regression machine-learning model to predict T_{50} (the temperature at which the intensity of the phosphor is reduced by 50% relative to its low-temperature emission intensity) of Eu³⁺ phosphors evaluated with leave-one-out cross-validation against experimentally measured T_{50} . The dashed black line shows the ideal 1:1 line. The model has a coefficient of determination of $r^2 = 0.71$ and a mean absolute error (MAE) of 31 K. f, The machine-learning model evaluated in part e successfully identified five new thermally robust phosphors each with an experimentally determined T_{50} above 420 K. The dashed line indicates 50% of the room temperature emission intensity as a guide to the eye. ΔR , the parabola offset between the ground and excited state; a.u., arbitrary unit; E_{α} , band gap; R, the metal-ligand distance; RE, rare earth; v_n , vibrational states of the ground state; v_n' , vibrational states of the excited state. Parts a and b adapted with permission from ref. 104, Copyright 2017 American Chemical Society. Parts c and d adapted with permission from ref. 48. Copyright 2020 American Chemical Society. Parts e and f adapted with permission from ref. 74, Copyright 2020 American Chemical Society.

an electron from the rare-earth excited $5d_1$ energy level to the conduction band 73 . The probability of this quenching mechanism occurring depends entirely on the position of the rare-earth 5d orbitals and the distance between the $5d_1$ orbital relative to the edge of the conduction band. Conversely, excited-state crossover relaxation involves large shifts in the excited state potential energy surface relative to the ground state potential energy surface, ΔR , which creates a crossover point between these two surfaces that acts as a non-radiative relaxation pathway 59 (Fig. 6b).

Creating a computational model to predict the thermal stability of a phosphor requires thermally induced photoionization and excited-state crossover relaxation to be considered as competing processes. One example of such a computational model is the dual-barrier thermal quenching model, which was developed using first-principles calculations⁴⁸. First, ab initio molecular dynamics simulations were performed on 29 known phosphors at 300 K (approximating ambient conditions) and 500 K (the upper temperature limit experienced by a phosphor in pc-LEDs). Information about the local coordination environment of the rare-earth activator ion was then extracted at each temperature to establish a parameter called the activator environment distribution (AED)⁴⁸. The AED is derived by determining the total number of times an activator has a particular coordination number. The difference between the AED at 300 K and 500 K (ΔAED) was then calculated for each system and thermally robust phosphors were found to exhibit a minimal ΔAED⁴⁸. The dual-barrier model then combines $\triangle AED$ with the thermal ionization barrier, E_{av}^{i} which depends on the host band gap (E_g) , centroid shift (ε_c) and crystal field splitting (ε_{cfs}), to predict the magnitude of thermal quenching⁴⁸. This model was used to construct a design map to identify thermally robust Ce³⁺-substituted and Eu²⁺-substituted phosphors. Eu²⁺substituted phosphors with a thermal quenching less than 20% (quantified as a percentage decrease in the temperature-dependent emission intensity relative to the low-temperature emission intensity) can thus be developed by using host structures with $\triangle AED < 0.05$ and $E_a^i > 0.82$ eV (Fig. 6c). A second map to screen for phosphors with low thermal quenching based on the rare-earth substitutional environment was created by plotting E_a^i against E_g , the average activator-ligand bond length (l_{avg}) and average cation electronegativity (χ_{avg}) (Fig. 6d). At sufficiently large band gaps $(E_g > 4 \text{ eV})$, the E_a^i necessary for low thermal quenching can be achieved for a wide range of l_{avg} and χ_{avg} . This tool, while successful at identifying the metrics that guide thermal stability, is one, albeit computationally expensive approach, to expedite phosphor discovery.

Finally, machine learning can be used to directly predict the T_{50} of activators that undergo $4f^n \leftrightarrow 4f^n$ transitions, in which case multiphonon relaxation is typically the dominant quenching mechanism. The thermal quenching temperature of Eu^{3+} -substituted phosphors was predicted by developing an SVR-based machine learning model on the basis of an initial training set of $134\ T_{50}$ values⁷⁴. The model achieved good correlation between the predicted and experimentally observed T_{50} values ($r^2=0.71$, mean absolute error = 31 K) (Fig. 6e). This model predicted the T_{50} of more than 1,000 potential oxide phosphor hosts and was used to identify five new Eu^{3+} -substituted phosphors with T_{50} values above 423 K (Fig. 6f). A similar machine-learning model to predict T_4 could also be developed to meet the recommendation of the US DOE that a phosphor loses only 4% of the room temperature emission intensity at 423 K.

Alternatively, it is also reasonable to aim for phosphors with $T_{50} \approx 523$ K (250 °C), given the typical 'inverse S' shape of the relationship

between the normalized, integrated emission intensity of phosphors that undergo $4f^{n-1}5d^1\leftrightarrow 4f^n5d^0$ transitions and temperature. Machine learning could possibly be applied to rapidly identify thermally robust phosphors that undergo $4f^{n-1}5d^1\leftrightarrow 4f^n5d^0$ transitions by predicting these inverse S curves. It is worth noting that phosphors that contain defects because of aliovalent substitution might not exhibit an inverse S curve. These defect states trap photons, which are eventually thermally depopulated 75. This depopulation causes an increase in the integrated emission intensity as a function of temperature, which gives the illusion of thermal stability. Instead, temperature-dependent PLQY measurements should be conducted to investigate the thermal stability of a material. Temperature-dependent lifetime measurements could also be conducted; however, the presence of the defects might induce persistent luminescence, which can affect the resulting analysis 10,76 .

Outlook and conclusions

Substantial progress has been made in developing synthetic and data-driven methodologies to rapidly identify phosphors that are suitable for commercial applications. However, there are still areas that require attention to facilitate the discovery of phosphors that meet the remaining requirements.

Strong LED absorption

As mentioned earlier, the shape, width and location of the excitation (absorption) band of a phosphor are crucial because they determine its compatibility with violet or blue LEDs. The most prevalent limitation of phosphors reported in the literature today is that their excitation bands do not cover the LED wavelengths of interest ($\lambda_{\text{em,max}} = 400 \text{ nm}$ and $\lambda_{\text{em,max}}$ = 450 nm). Therefore, it is imperative to understand how to ensure the absorption of LED radiation in phosphors. The absorption spectrum of inorganic phosphors is measured by converting a diffuse reflectance spectrum using the Kubelka-Munk transformation, but this approach does not provide an absorption coefficient. Measuring the absorption coefficients of powder samples is critical to quantify absorption; however, such measurements are not trivial. Techniques to measure and report the particle size-dependent absorption coefficient are needed to ensure that phosphors meet the minimum requirements of $\alpha > 50$ cm⁻¹ and to provide a metric to compare the absorption of new materials. Finally, phosphor droop, or the decrease in EQE as the LED power density increases, has become a research focus owing to improvements in the overall power density of high-power In_{1-x}Ga_xN LEDs and laser diode technologies. Methods to mitigate possible excited state absorption or cross-relaxation by Förster or Dexter transfer quenching pathways should also be developed further⁷⁷. Additional experimental studies focused on the relationship between the absorption and crystal chemistry of a phosphor would undoubtedly be helpful.

Advances in DFT and access to high-performance computing clusters have provided some assistance in calculating the absorption spectrum of a phosphor before synthesis. A simple linear harmonic oscillator has been used to calculate the energy and relative oscillator strengths of the $4f \rightarrow 5d$ transitions by modelling rare-earth-centred defect clusters within an optimized host crystal structure. Complete active-space self-consistent-field and second-order many-body perturbation theory calculations based on quantum chemical wave functions can then be performed to obtain the estimated energy of the derived $4f \rightarrow 5d$ transitions. This process, as briefly described here, might seem simple. But in reality, these calculations are computationally demanding *8. Furthermore, these calculations are generally limited to Ce³+ because it is difficult to model the complex excited state

manifold of $\mathrm{Eu^{2+}}$ owing to the 4f' octet ground state of $\mathrm{Eu^{2+}}$ (ref. 79). These calculations are also semi-quantitative and provide supplementary information to aid in understanding the observed optical properties of a phosphor a posteriori, but often show moderate deviations from experimental data. Thus, although this computational approach is valuable, high-throughput complete active-space self-consistent-field and second-order many-body perturbation theory calculations would be computationally expensive, making it impractical to use as a method to uncover the structure–composition trends that guide excitation band shape and position of phosphors $^{80-82}$.

Progress has also been made by using data science to predict the excitation band edge wavelength; however, it is challenging to construct such a model⁸³. In one example, the data set extracted from the literature used to train the model had to be restricted to host structures that only contain one crystallographic site for Eu²⁺ substitution and where the rare-earth concentration was optimized. This restriction was done in an attempt to ensure that the most accurate excitation band edge wavelength values were obtained. These strict criteria narrowed the training data set to only 91 phosphors. The small training data set meant that the number of features that the machine-learning model could use had to be minimized to prevent overfitting. The features used mainly described the rare-earth local structure, but there was also difficulty in obtaining reliable descriptors for crystal field splitting data, which can influence the position and shape of the excitation spectrum of a phosphor. The combination of these limitations led to an integrated machine-learning platform with moderate predictive power⁸³ ($r^2 = 0.53$). However, these findings are an exciting start to using data science to understand and eventually predict the excitation spectrum of a material.

Environmental stability

The development of phosphors for solid-state lighting needs to continue beyond achieving desired optical properties. To maximize the operational lifetime of pc-LED lighting devices, the phosphor must be able to withstand degradation from the high-intensity light and heat generated by the LED and the ambient moisture and solvents encountered during device fabrication^{2,5,14}. Additionally, the phosphors should remain robust to the harsh climates (high ambient temperatures and intense solar radiation) where these devices can be used^{8,4}. Each external stimulus increases the probability of non-radiative relaxation occurring in the phosphor, which can decrease the PLQY of a phosphor and therefore decrease the overall energy efficiency of the device. Moreover, phosphors degrading at different rates within an LED package can induce shifts in the emission band position, shape and FWHM, which can alter the perceived colour of the white light source. Under extreme cases, these stimuli can also cause the material to irreversibly decompose.

Most new phosphor publications do not discuss how the chemical, structural or optical properties of the material respond to moisture or elevated temperatures. The efficiency of a phosphor with respect to high incident light flux is also often overlooked despite the advent of laser-driven lighting, which can have light fluxes >100 W cm⁻² (ref. 85). This oversight is surprising considering that there are many simple laboratory experiments that can reveal some initial chemical stability issues of a material such as prolonged annealing at elevated temperatures or dispersing the powder in water and examining the structural and optical properties of the phosphors pre-treatment and post-treatment. The optical response to incident light flux of a phosphor can be determined by measuring the relative intensity loss as a function of time under constant laser irradiation⁸⁵.

The change in the optical properties of a phosphor upon exposure to these external stimuli should be <5% over the course of the lifetime of a LED package⁸⁵. This requirement is especially crucial because the colour of the light produced by LED packages can shift if the phosphors degrade during operation. Chromatic shifts of phosphors and white light sources can be investigated using the 1976 CIE (Commission Internationale de l'Eclairage, or International Commission for Illumination) $L^*u^*v^*$ colour space. In this colour space, L^* refers to perceptual lightness (light versus dark) and u^* and v^* refer to tristimulus values, which are used to calculate (u', v') coordinates that can be plotted on the colour space diagram. The 1976 CIE $L^*u^*v^*$ colour space, unlike the CIE 1931 XYZ colour space, is perceptually uniform, meaning that the distance between the initial and final (u', v') coordinates corresponds to a proportional shift in observed colour⁹. One of the best practices to quantify a chromatic shift is to calculate the distance between the ambient colour point (u'_{init}, v'_{init}) and the average of all colour points measured as a function of temperature or time under certain environmental conditions (u'_{avg}, v'_{avg}) ,

$$\Delta u' \Delta v' = \sqrt{(u'_{avg.} - u'_{init.})^2 + (v'_{avg.} - v'_{init.})^2}.$$
 (5)

Ensuring that the colour shift of an LED package throughout its lifetime is indistinguishable requires confirming that $\Delta u' \Delta v'$ and all of the stimuli-dependent colour coordinates lie within a MacAdam ellipse of a targeted step size, in which one step size represents one standard deviation from the average ^{15,86}. Although the American National Standards Institute suggests that chromaticity differences should be confined within a 7-step MacAdam ellipse for solid-state lighting devices, industries typically require chromaticity differences in commercial pc-LEDs to fall within a ≤4-step MacAdam ellipse over their operational lifetime^{87,88}. A better target is to limit the chromaticity shifts of individual phosphors to a 1-step MacAdam ellipse. This goal has already been achieved in industry in the optimization of a phosphor blend containing Y₂Al₅O₁₂:Ce³⁺ and K₂SiF₆:Mn⁴⁺ from a 4-step MacAdam ellipse under 1.000 h of typical operation to a 1-step MacAdam ellipse after 4.000 h of operation⁸⁵. The environmental stability of phosphors is not often considered; therefore, we encourage researchers to begin performing this type of analysis to understand and control the overall stability of a material.

Building a phosphor discovery pipeline

There have been substantial strides in the development of tools to target specific optical properties in inorganic phosphors. Unfortunately, it is unlikely that a single approach or research tool will be developed that is capable of discovering phosphors that possess all six of the desired properties (Fig. 7). Therefore, it is important to prioritize the targeted properties. These properties can be split into three groups – the first group contains properties that are non-negotiable for solid-state lighting, namely, strong LED absorption, an appropriate emission colour and a high PLQY. The requirement for a phosphor to be able to absorb blue (or violet) LED emitted light is primarily cost-driven. The LED chip accounts for >50% of the cost of an LED package, even after decades of optimizing their synthesis and energy efficiency⁴. Conversely, the phosphor accounts for ~8% of package costs; therefore, it is far cheaper to ensure compatibility by developing a phosphor that strongly absorbs LED radiation rather than developing efficient LEDs that emit at the exact excitation wavelength suitable for a phosphor⁴. Unfortunately, the majority of new phosphors discovered only absorb in the ultraviolet range. Therefore, the step that is slowing down the discovery

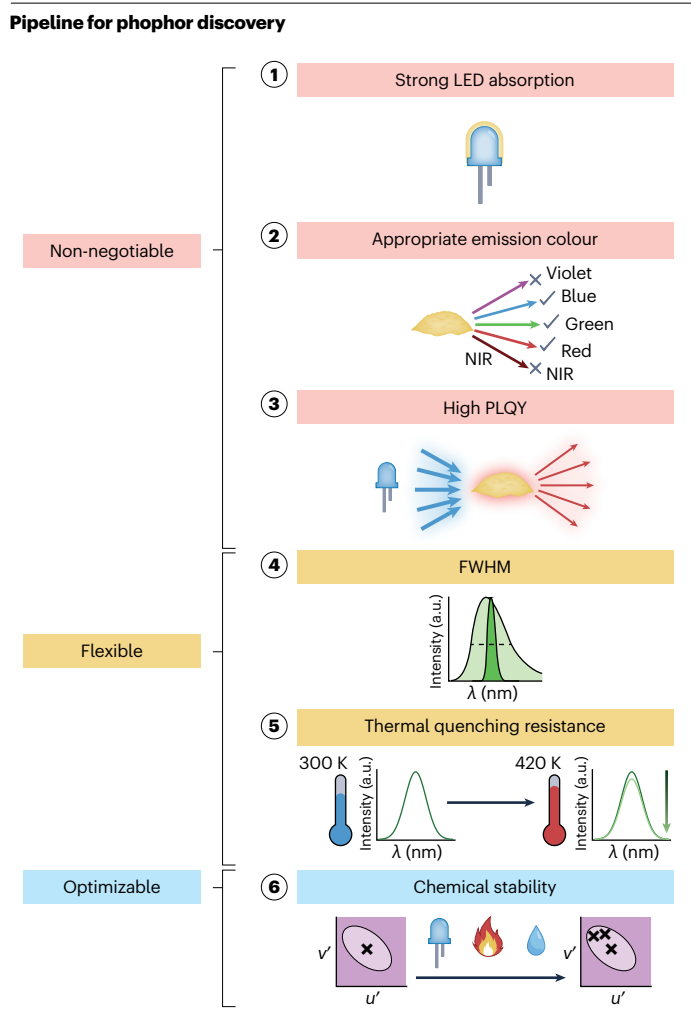


Fig. 7 | A phosphor discovery pipeline. Discovering a single phosphor that immediately possesses all of the desirable optical properties is non-trivial; therefore, we suggest that these optical properties should be prioritized as follows. (1) Strong light-emitting diode (LED) absorption: phosphors must strongly absorb blue or violet light emitted by an LED. (2) Appropriate emission colour: to maximize efficiency phosphors must not produce violet or near-infrared (NIR) light. (3) High photoluminescent quantum yield (PLQY): phosphors must convert nearly all of the incident LED light into an emission of a desirable colour. (4) Full width at half maximum (FWHM): the width of the emission should be narrow enough to minimize lost photons while being wide enough to provide high colour quality; the optimal FWHM value depends on the desired emission wavelength. (5) Thermal quenching resistance: the decrease in the intensity of the phosphor emission caused by an increase in temperature should be minimized. (6) Chemical stability: it is desirable to minimize the chromatic shift that occurs following exposure to light, heat or humidity. These properties can be further split into three groups: non-negotiable, flexible and those most likely to be optimized. a.u., arbitrary unit.

of new phosphors is also the first step in the pipeline. This limitation further reinforces the need for data-driven methods to expedite the process of discovering phosphors that strongly absorb LED radiation. Emission colour also often precludes many phosphors from being used. Phosphors that produce violet or near-infrared emission will never be

used in pc-LEDs for general illumination and display lighting because they cannot down-convert LED radiation or they emit outside the visible region¹¹. Finally, phosphors must have a high PLQY to overcome the inherent Stokes loss and maximize photon emission⁸⁹. Achieving these three properties in a single phosphor ensures that pc-LED costs are minimized and energy efficiency is prioritized.

The second group of required properties contains FWHM and thermal quenching resistance, which are properties that have a certain degree of flexibility. The FWHM should be tuned to find an appropriate balance between efficacy and colour quality¹². Therefore, the desired FWHM of a phosphor can vary depending on $\lambda_{\rm em,max}$. If $\lambda_{\rm em,max}$ is near the perceptible limit of the human eye, an FWHM of 30 nm is required to minimize spillover emission4. Blue-emitting and green-emitting phosphors can have more flexibility in their emission FWHM than red-emitting phosphors because there is less risk of losing photons to the ultraviolet. A broad FWHM can also improve colour-rendering capabilities of a device 12 . It is important to note that the FWHM ≈ 30 nm goal across the visible spectrum prioritizes efficacy over colour quality. The amount of thermal quenching experienced by a phosphor is also somewhat flexible and application-dependent. Thermally robust phosphors are necessary when the pc-LED device architecture creates contact between the phosphor and LED chip, whereas remote phosphor geometries limit the need for thermally robust optical properties $^{90-92}$. Optimizing the heat sinks used within the pc-LED package can also help to dissipate the heat⁹³ and reduce the temperatures experienced by the phosphor. Finally, the thermal quenching expectations are different for LEDs used in displays compared with those used in general lighting applications. The flexibility in the required FWHM and thermal stability of a phosphor allow for a wider range of materials to be considered for commercial pc-LEDs.

The final category, which contains chemical stability, is of lower priority than the previous two groups because this property can often be improved through post-processing techniques. For example, K₂SiF₆:Mn⁴⁺ is prone to hydrolysis and light-based damage, which induce chromatic instabilities⁸⁵. Optical spectroscopy was vital in identifying light-based damage as the primary contributor to these reliability issues. By improving the composition, synthesis and processing of a phosphor, the chromatic shift of K₂SiF₆:Mn⁴⁺ was confined to a 1-step MacAdam ellipse⁸⁵. There are also many examples in which the chemical stability of a phosphor has been improved by applying a coating to the phosphor particles. For example, applying an Al₂O₃ coating to Sr₂Si₅N₈:Eu²⁺ and K₂GeF₆:Mn⁴⁺ using atomic layer deposition prevented the phosphors from undergoing thermal and moisture degradation, respectively 94,95. Other coatings, such as SiO₂, C, octadecyltrimethoxysilane and oleic acid, can also improve the chemical stability of phosphors 96-99. Nevertheless, the development of models to identify and mitigate the mechanisms responsible for chemical instability would substantially reduce the time taken to integrate new phosphors into pc-LEDs.

Advances in robotics and automated high-throughput synthesis provide an exciting opportunity to down-select materials following this workflow with the exact optical properties required to improve the performance of pc-LEDs^{100,101}. For example, high-throughput synthesis can be conducted with earth-abundant precursors and a cost-effective synthesis approach to create a powder library and to perform experimental screening using the single-particle diagnosis. Such approaches will accelerate the discovery of phosphors that can be excited by blue or violet LED radiation and produce a desirable emission colour (spectrum). Automated high-throughput synthesis is already being applied to synthesize and identify phosphors. Indeed, a

rapid automated materials synthesis instrument capable of performing automated manufacturing, cleaning and ceramic printing was used to identify highly efficient Eu³⁺-substituted phosphors¹⁰². Yet, there are some challenges with robotic automation. Namely, synthesis can involve multiple steps. For example, some systems can only form following multiple intermittent grinding steps. Such processes are difficult to automate, meaning that it is possible that new phases could be overlooked and that the searchable phase space is limited¹⁰². Another challenge involves validating the compatibility of corrosive precursors with the automation instruments. These specific challenges fall into a broader category of how automated synthesis differs from small-scale (1–5 g) materials synthesis and the effect of this difference on phase space screening and eventual scale-up. A different approach can also be conducted by applying a heuristics optimization, in which the objective functions can be chosen to target phosphors with a specific emission colour under strong LED absorption. Novel phosphor compositions identified with this approach that exhibit a desirable emission colour under LED excitation can be considered as potential candidates for continued exploration. Continuing through the pipeline, machine-learning models can be trained to predict the PLQY of particles identified in high-throughput experiments, enabling further down-selection of systems with the non-negotiable target properties. Similarly, machine-learning models capable of predicting the FWHM and temperature-dependent optical properties can also be used to continue narrowing the compositional space of interest, depending on the desired application and device architecture of the package. Finally, chemical stability can be addressed in systems that maximize these non-negotiable and flexible properties through data-driven accelerated ageing tests to identify opportunities for maximizing phosphor reliability. We envisage that prioritizing this workflow and using a combination of experimental and data-driven science will be the best approach to accelerate the identification and development of phosphors with clear potential for applications in commercial solid-state lighting devices.

Conclusion

Pc-LED technology has had a tremendous societal impact by reducing global energy consumption. The nearly unlimited combinations of host crystal structures and activators have resulted in new reports of phosphors being published almost daily. As many of these phosphors lack the most basic optical property requirements, crystal-chemical design rules and data-driven tools have been developed to facilitate the discovery of robust phosphors. These tools have expedited the discovery of phosphors with an exact emission colour, high efficiency, a narrow FWHM or thermally robust emission. Tools to target phosphors with strong LED absorption that are also chemically stable must be developed to further reduce the time taken to transition a phosphor from the laboratory to a commercial pc-LED device. Identifying a single novel phosphor that possesses all the required optical properties is still non-trivial. Therefore, we envisage that the future of phosphor discovery will rely on advances in automated chemistry to down-select and converge upon a single material by following a workflow that prioritizes the non-negotiable optical properties over those that have a high probability of being improved upon post-processing. These tools offer an exciting opportunity to rapidly identify transformative phosphors with the potential to improve the performance of pc-LEDs across various applications such as next-generation horticultural and vertical farming, human-centric lighting, near-infrared LED lighting and beyond.

Published online: 09 October 2023

References

- United Nations Environment Programme. The Rapid Transition to Energy Efficient Lighting: An Integrated Policy Approach. UNEP https://wedocs.unep.org/20.500.11822/ 8468 (2013).
- Pust, P., Schmidt, P. J. & Schnick, W. A revolution in lighting. Nat. Mater. 14, 454–458 (2015).
- George, N. C., Denault, K. A. & Seshadri, R. Phosphors for solid-state white lighting. Annu. Rev. Mater. Res. 43, 481–501 (2013).
- Morgan, P. et al. 2022 Solid-State Lighting R&D Opportunities. US Department of Energy Office of Scientific and Technical Information https://doi.org/10.2172/1862626 (2022).
- McKittrick, J. & Shea-Rohwer, L. E. Review: down conversion materials for solid-state lighting. J. Am. Ceram. Soc. 97, 1327–1352 (2014).
- Meyer, J. & Tappe, F. Photoluminescent materials for solid-state lighting: state of the art and future challenges. Adv. Opt. Mater. 3, 424–430 (2015).
- Luo, X. & Xie, R.-J. Recent progress on discovery of novel phosphors for solid state lighting. J. Rare Earths 38, 464–473 (2020).
- lighting. *J. Rare Earths* **38**, 464–473 (2020).

 8. Zhuo, Y. & Brgoch, J. Opportunities for next-generation luminescent materials through
- artificial intelligence. *J. Phys. Chem. Lett.* **12**, 764–772 (2021).

 9. Hariyani, S. & Brgoch, J. Spectral design of phosphor-converted LED lighting guided
- by color theory. Inorg. Chem. **61**, 4205–4218 (2022).

 10. Hariyani, S. & Brgoch, J. Advancing human-centric LED lighting using Na₂MgPO₄F:Eu²⁺.
- ACS Appl. Mater. Interfaces 13, 16669–16676 (2021).
- Lumileds. Narrow Red Phosphor Technology. Lumileds https://lumileds.com/wp-content/ uploads/files/WP32.pdf (2016).
- Ohno, Y. Color rendering and luminous efficacy of white LED spectra. Proc. SPIE Int. Soc. Opt. Eng. 5530, 88–98 (2004).
- National Research Council, Division on Engineering and Physical Sciences, Board on Energy and Environmental Systems & Committee on Assessment of Solid-state Lighting. Assessment of Advanced Solid-State Lighting (The National Academies Press, 2013).
- Murphy, J. E., Garcia-Santamaria, F., Setlur, A. A. & Sista, S. 62.4: PFS, K₂SiF₈:Mn⁴: the red-line emitting LED phosphor behind GE's TriGain Technology™ platform. SID Int. Symp. Dig. Tec. 46, 927-930 (2015).
- MacAdam, D. L. Specification of small chromaticity differences. J. Opt. Soc. Am. 33, 18–26 (1943).
- Dorenbos, P. Crystal field splitting of lanthanide 4fⁿ⁻¹5d-levels in inorganic compounds. J. Alloy. Compd. 341, 156–159 (2002).
- Xia, Y. et al. Crystal structure evolution and luminescence properties of color tunable solid solution phosphors Ca_{2*x}La_{8-x}(SiO₄)_{6-x}(PO₄)_xO₂:Eu^{2*}. Dalton Trans. 45, 1007–1015 (2016).
- Jiang, L. et al. Multiobjective machine learning-assisted discovery of a novel cyan-green garnet: Ce phosphors with excellent thermal stability. ACS Appl. Mater. Interfaces 14, 15426-15436 (2022).
- Lai, S., Zhao, M., Qiao, J., Molokeev, M. S. & Xia, Z. Data-driven photoluminescence tuning in Eu²⁺-doped phosphors. *J. Phys. Chem. Lett.* 11, 5680–5685 (2020).
- van Uitert, L. G. An empirical relation fitting the position in energy of the lower d-band edge for Eu²⁺ or Ce³⁺ in various compounds. J. Lumin. 29, 1–9 (1984).
- Park, W. B., Singh, S. P., Kim, M. & Sohn, K.-S. Phosphor informatics based on confirmatory factor analysis. ACS Comb. Sci. 17, 317–325 (2015).
- Wang, Q. et al. Crystal structure and photoluminescence properties of Eu²⁺-activated Ba₂LiB₅O₁₀ phosphors. Opt. Commun. 284, 5315–5318 (2011).
- Sonekar, R., Omanwar, S. & Moharil, S. Combustion synthesis and photoluminescence of Eu²⁺ doped BaB8013. *Indian J. Pure Appl. Phys.* 47, 441–443 (2009).
- Lee, J.-W. et al. Metaheuristics-assisted combinatorial screening of Eu²⁺-doped Ca–Sr–Ba–Li–Mg–Al–Si–Ge–N compositional space in search of a narrow-band green emitting phosphor and density functional theory calculations. *Inorg. Chem.* 56, 9814–9824 (2017).
- Park, W. B., Singh, S. P. & Sohn, K.-S. Discovery of a phosphor for light emitting diode applications and its structural determination, Ba(Si,Al)₅(O,N)₈:Eu²⁺. J. Am. Chem. Soc. 136, 2363–2373 (2014).
- Strobel, P. et al. Narrow-band green emitting nitridolithoalumosilicate Ba[Li₂(Al₂Si₂) N₆]:Eu²⁺ with framework topology whj for LED/LCD-backlighting applications. Chem. Mater. 27. 6109–6115 (2015).
- Park, W. B., Singh, S. P., Yoon, C. & Sohn, K.-S. Combinatorial chemistry of oxynitride phosphors and discovery of a novel phosphor for use in light emitting diodes, Ca₁₅Ba₀₅Si ₅N₆O₃:Eu²⁺. J. Mater. Chem. C 1, 1832–1839 (2013).
- Park, W. B., Shin, N., Hong, K.-P., Pyo, M. & Sohn, K.-S. A new paradigm for materials discovery: heuristics-assisted combinatorial chemistry involving parameterization of material novelty. Adv. Funct. Mater. 22, 2258–2266 (2012).
- Kulshreshtha, C., Sharma, A. K. & Sohn, K.-S. Search for new red phosphors using genetic algorithm-assisted combinatorial chemistry. J. Comb. Chem. 10, 421–425 (2008).
- Singh, S. P., Kim, M., Park, W. B., Lee, J.-W. & Sohn, K.-S. Discovery of a red-emitting Li₃RbGe₈O₁₈:Mn⁴⁺ phosphor in the alkali-germanate system: structural determination and electronic calculations. *lnorg*. Chem. 55, 10310–10319 (2016).
- Takeda, T., Hirosaki, N., Funahashi, S. & Xie, R.-J. New phosphor discovery by the single particle diagnosis approach. *Mater. Discov.* 1, 29–37 (2015).
- Zhang, Y. et al. Realizing red/orange emission of Eu²⁺/Ce³⁺ in La_{26-x}Sr_xSi₄₁O_{x+}N_{80-x} (x = 12.72–12.90) phosphors for high color rendition white LEDs. J. Mater. Chem. C 8, 13458–13466 (2020).
- Hirosaki, N., Takeda, T., Funahashi, S. & Xie, R.-J. Discovery of new nitridosilicate phosphors for solid state lighting by the single-particle-diagnosis approach. Chem. Mater. 26, 4280–4288 (2014).

- Takeda, T., Hirosaki, N., Funahshi, S. & Xie, R.-J. Narrow-band green-emitting phosphor Ba₂LiSi₇AlN₁₂:Eu²⁺ with high thermal stability discovered by a single particle diagnosis approach. Chem. Mater. 27, 5892–5898 (2015).
- 35. Wang, C.-Y. et al. New deep-blue-emitting Ce-doped A_{4-m}B_nC_{19+2m}X_{29+m} (A = Sr, La; B = Li; C = Si, Al; X = O, N; O ≤ m ≤ 1; O ≤ n ≤ 1) phosphors for high-color-rendering warm white light-emitting diodes. ACS Appl. Mater. Interfaces 11, 29047–29055 (2019).
- Wong, K.-L., Bünzli, J.-C. G. & Tanner, P. A. Quantum yield and brightness. J. Lumin. 224, 117256 (2020).
- Feldmann, C., Jüstel, T., Ronda, C. R. & Wiechert, D. U. Quantum efficiency of down-conversion phosphor LiGdF4:Eu. J. Lumin. 92, 245–254 (2001).
- Fan, B., Chlique, C., Merdrignac-Conanec, O., Zhang, X. & Fan, X. Near-infrared quantum cutting material Er³⁺/Yb³⁺ doped La₂O₂S with an external quantum yield higher than 100%. J. Phys. Chem. C 116. 11652–11657 (2012).
- Zhong, Y. et al. Pyrophosphate phosphor solid solution with high quantum efficiency and thermal stability for efficient LED lighting. iScience 23, 100892 (2020).
- Dexter, D. L. & Schulman, J. H. Theory of concentration quenching in inorganic phosphors. J. Chem. Phys. 22, 1063–1070 (2004).
- Rohwer, L. S. & Martin, J. E. Measuring the absolute quantum efficiency of luminescent materials. J. Lumin. 115, 77–90 (2005).
- Zhuo, Y., Mansouri Tehrani, A., Oliynyk, A. O., Duke, A. C. & Brgoch, J. Identifying an
 efficient, thermally robust inorganic phosphor host via machine learning. *Nat. Commun.*9, 4377 (2018).
- 43. George, N. C. et al. Local environments of dilute activator ions in the solid-state lighting phosphor Y_{3-x} Ce_xAl₅O₁₂. Chem. Mater. **25**, 3979–3995 (2013).
- Guo, C., Xu, Y., Ren, Z. & Bai, J. Blue-white-yellow tunable emission from Ce³⁺ and Eu²⁺ co-doped BaSiO₃ phosphors. J. Electrochem. Soc. 158, J373 (2011).
- Brgoch, J., DenBaars, S. P. & Seshadri, R. Proxies from ab initio calculations for screening efficient Ce³⁺ phosphor hosts. *J. Phys. Chem. C* 117, 17955–17959 (2013).
- Hariyani, S., Duke, A. C., Krauskopf, T., Zeier, W. G. & Brgoch, J. The effect of rare-earth substitution on the Debye temperature of inorganic phosphors. *Appl. Phys. Lett.* 116, 051901 (2020)
- Hermus, M. & Brgoch, J. Phosphors by design: approaches toward the development of advanced luminescent materials. Electrochem. Soc. Interface 24, 55–59 (2015).
- 48. Amachraa, M. et al. Predicting thermal quenching in inorganic phosphors. *Chem. Mater.* **32**, 6256–6265 (2020).
- Jain, A. et al. Commentary: the materials project: a materials genome approach to accelerating materials innovation. APL Mater. 1, 011002 (2013).
- Zhong, J. et al. Closing the cyan gap toward full-spectrum LED lighting with NaMgBO₃:Ce³⁺. Chem. Mater. 32, 882–888 (2020).
- Im, W. B. et al. Sr_{2,975-x}Ba_xCe_{0,025}AlO₄F: a highly efficient green-emitting oxyfluoride phosphor for solid state white lighting. *Chem. Mater.* 22, 2842–2849 (2010).
- Hariyani, S. & Brgoch, J. Local structure distortion induced broad band emission in the all-inorganic BaScO₂F:Eu²⁺ perovskite. Chem. Mater. 32, 6640–6649 (2020).
- You, S., Zhuo, Y., Chen, Q., Brgoch, J. & Xie, R.-J. Dual-site occupancy induced broadband cyan emission in Ba₂CaB₂Si₄O₁₄:Ce³⁺. J. Mater. Chem. C 8, 15626–15633 (2020).
- Ha, J. et al. An integrated first principles and experimental investigation of the relationship between structural rigidity and quantum efficiency in phosphors for solid state lighting. J. Lumin. 179, 297–305 (2016).
- Duke, A. C., Finley, E., Hermus, M. & Brgoch, J. Yellow-green luminescence and extreme thermal quenching in the Sr_eM₂Al₄O₁₅:Eu²⁺ (M = Y, Lu, Sc) phosphor series. Solid State Sci. 60, 108–113 (2016).
- Brik, M. G., Srivastava, A. M. & Popov, A. I. A few common misconceptions in the interpretation of experimental spectroscopic data. Opt. Mater. 127, 112276 (2022).
- 57. Lakowicz, J. R. *Principles of Fluorescence Spectroscopy* 3rd edn 53–54 (Springer, 2008).
- Mooney, J. & Kambhampati, P. Get the basics right: Jacobian conversion of wavelength and energy scales for quantitative analysis of emission spectra. J. Phys. Chem. Lett. 4, 3316–3318 (2013).
- 59. Blasse, G. & Grabmaier, B. C. Luminescent Materials 72-84 (Springer-Verlag, 1994).
- Li, S. et al. Data-driven discovery of full-visible-spectrum phosphor. Chem. Mater. 31, 6286–6294 (2019).
- Strobel, P. et al. Luminescence of an oxonitridoberyllate: a study of narrow-band cyan-emitting Sr[Be₆ON₄]:Eu²⁺. Chem. Mater. 30, 3122–3130 (2018).
- Strobel, P., Maak, C., Weiler, V., Schmidt, P. J. & Schnick, W. Ultra-narrow-band blue-emitting oxoberyllates AELi₂[Be₄O₆]:Eu²⁺ (AE=Sr, Ba) paving the way to efficient RGB pc-LEDs. Angew. Chem. Int. Ed. 57, 8739–8743 (2018).
- Wendl, S. et al. Nitridophosphate-based ultra-narrow-band blue-emitters: luminescence properties of AEP₈N₁₄:Eu²⁺ (AE=Ca, Sr, Ba). Chem. Eur. J. 26, 7292–7298 (2020).
- Li, C. et al. Narrow-band blue emitting nitridomagnesosilicate phosphor Sr₈Mg₇Si₉N₂₂:Eu²⁺ for phosphor-converted LEDs. Chem. Commun. 54, 11598–11601 (2018).
- Zhuo, Y., Hariyani, S., Zhong, J. & Brgoch, J. Creating a green-emitting phosphor through selective rare-earth site preference in NaBaB₉O₁₅:Eu²⁺. Chem. Mater. 33, 3304–3311 (2021).
- Chen, Y.-J., Cao, F.-B., Tian, Y.-W., Xiao, L.-J. & Li, L.-K. Optimized photoluminescence by charge compensation in a novel phosphor system. *Phys. B* 405, 435–438 (2010).
- 67. Duke, A. C., Hariyani, S. & Brgoch, J. Ba $_3$ Y $_2$ B $_6$ O $_{15}$:Ce 3* a high symmetry, narrow-emitting blue phosphor for wide-gamut white lighting. *Chem. Mater.* **30**, 2668–2675 (2018).
- Pust, P. et al. Narrow-band red-emitting Sr[LiAl₃N₄]:Eu²⁺ as a next-generation LED-phosphor material. Nat. Mater. 13, 891–896 (2014).

- Pust, P. et al. Group (III) nitrides M[Mg₂Al₂N₄] (M = Ca, Sr, Ba, Eu) and Ba[Mg₂Ga₂N₄] structural relation and nontypical luminescence properties of Eu²⁺ doped samples. Chem. Mater. 26, 6113–6119 (2014).
- García-Fuente, A. et al. Properties design: prediction and experimental validation of the luminescence properties of a new Eu^{II}-based phosphor. Chem. Eur. J. 24, 16276–16281 (2018).
- Henderson, B. & Imbusch, G. F. Optical Spectroscopy of Inorganic Solids 199–208 (Clarendon Press 1989).
- Brinkley, S. E. et al. Robust thermal performance of Sr₂Si₅N₈:Eu²: an efficient red emitting phosphor for light emitting diode based white lighting. Appl. Phys. Lett. 99, 241106 (2011).
- Dorenbos, P. Thermal quenching of Eu²⁺ 5d-4f luminescence in inorganic compounds. J. Phys. Condens. Matter 17, 8103–8111 (2005).
- Zhuo, Y., Hariyani, S., Armijo, E., Abolade Lawson, Z. & Brgoch, J. Evaluating thermal quenching temperature in Eu³⁺-substituted oxide phosphors via machine learning. ACS Appl. Mater. Interfaces 12, 5244–5250 (2020).
- Garlick, G. F. J. & Gibson, A. F. The electron trap mechanism of luminescence in sulphide and silicate phosphors. Proc. Phys. Soc. 60, 574 (1948).
- Müller, M. & Jüstel, T. On the luminescence and energy transfer of white emitting Ca₃Y₂(Si₃O₉)₂:Ce^{3*},Mn^{2*} phosphor. J. Lumin. 155, 398–404 (2014).
- Shchekin, O. B. et al. Excitation dependent quenching of luminescence in LED phosphors. Phys. Stat. Sol. Rapid Res. Lett. 10, 310–314 (2016).
- Wen, J. et al. First-principles study on structural, electronic, and spectroscopic properties of γ-Ca₂SiO₄:Ce³⁺ phosphors. J. Phys. Chem. A 119, 8031–8039 (2015)
- Huang, X. et al. Site occupation and spectral assignment in Eu²⁺-activated β-Ca₃(PO₄)₂type phosphors: insights from first-principles calculations. *Inorg. Chem.* 59, 16760–16768
 (2020).
- Zhong, J. et al. Combining experiment and computation to elucidate the optical properties of Ce³⁺ in Ba₅Si₈O₂₁. Phys. Chem. Chem. Phys. 22, 2327–2336 (2020).
- Wen, J. et al. Site occupation and 4f → 5d transitions of Ce³⁺ ions at mixed Ca²⁺/V³⁺ sites in CaYAlO₄: insights from first-principles calculations. J. Lumin. 216, 116726 (2019).
- Zhong, J. et al. Understanding the β-K₂CO₃-type Na(Na_{0.5}Sc_{0.5})BO₃:Ce³⁺ phosphor. ECS Solid. State Sci. Technol. 10, 096014 (2021).
- Park, C. et al. A data-driven approach to predicting band gap, excitation, and emission energies for Eu²⁺-activated phosphors. *Inorg. Chem. Front.* 8, 4610–4624 (2021).
- Wilkerson, A., Sullivan, G. P., Davis, R. G. & Safranek, S. Yuma Border Patrol Area Lighting Retrofit: Final LED System Performance Assessment of Trial and Full Installation. US Department of Energy Office of Scientific and Technical Information https://doi.org/ 10.2172/1437097 (2018).
- Hariyani, S. et al. From lab to lamp: understanding downconverter degradation in LED packages. J. Appl. Phys. 132, 190901 (2022).
- MacAdam, D. L. Visual sensitivities to color differences in daylight. J. Opt. Soc. Am. 32, 247–274 (1942).
- Narendran, N., Vasconez, S., Boyce, P. & Eklund, N. Just-perceivable color differences between similar light sources in display lighting applications. J. Illum. Eng. Soc. 29, 68–77 (2000).
- Jiang, R., Wang, Z., Wang, Q. & Dai, L. Multi-user sum-rate optimization for visible light communications with lighting constraints. J. Lightwave Technol. 34, 3943–3952 (2016).
- 89. Hartmann, P., Pachler, P., Payrer, E. & Tasch, S. in SPIE OPTO: Integrated Optoelectronic Devices (SPIE, 2009).
- Li, J. et al. Improvement in optical performance and color uniformity by optimizing the remote phosphor caps geometry for chip-on-board light emitting diodes. Solid State Electron. 126, 36–45 (2016).
- Perera, I. U. & Narendran, N. Analysis of a remote phosphor layer heat sink to reduce phosphor operating temperature. *Int. J. Heat Mass. Transf.* 117, 211–222 (2018).
- Chung, T. Y. et al. Study of temperature distribution within pc-WLEDs using the remote-dome phosphor package. IEEE Photon. J. 7, 1–11 (2015).
- Zheng, Z. et al. Enhanced heat dissipation of phosphor film in WLEDs by AlN-coated sapphire plate. IEEE Trans. Electron. Dev. 67, 3180–3185 (2020).
- Zhao, Y. et al. Enhanced thermal degradation stability of the Sr₂Si₂N₈:Eu²⁺ phosphor by ultra-thin Al₂O₃ coating through the atomic layer deposition technique in a fluidized bed reactor. J. Mater. Chem. C 7, 5772–5781 (2019).
- Zhao, Y. et al. Waterproof surface passivation of K₂GeF₆:Mn⁴⁺ by a dense Al₂O₃ layer via atomic layer deposition. J. Mater. Chem. C 10, 9867–9874 (2022).
- Zhang, F. et al. Silica coating enhances the stability of inorganic perovskite nanocrystals for efficient and stable down-conversion in white light-emitting devices. *Nanoscale* 10, 20131–20139 (2018).
- Liu, Y. et al. Achieving thermally stable and anti-hydrolytic Sr₂Si₅N₈:Eu²⁺ phosphor via a nanoscale carbon deposition strategy. Ceram. Int. 47, 3244–3251 (2021).
- Zhou, Y.-Y., Song, E.-H., Deng, T.-T. & Zhang, Q.-Y. Waterproof narrow-band fluoride red phosphor K₂TiF₆:Mn⁴⁺ via facile superhydrophobic surface modification. ACS Appl. Mater. Interfaces 10. 880–889 (2018).
- Arunkumar, P., Kim, Y. H., Kim, H. J., Unithrattil, S. & Im, W. B. Hydrophobic organic skin as a protective shield for moisture-sensitive phosphor-based optoelectronic devices. ACS Appl. Mater. Interfaces 9, 7232–7240 (2017).
- 100. Waltz, D. & Buchanan, B. G. Automating science. Science **324**, 43-44 (2009).
- Danielson, E. et al. A rare-earth phosphor containing one-dimensional chains identified through combinatorial methods. Science 279, 837–839 (1998).

- 102. Lin, T. et al. Rapid automated materials synthesis instrument: exploring the composition and heat-treatment of nanoprecursors toward low temperature red phosphors. J. Comb. Chem. 12, 383–392 (2010).
- Hariyani, S. & Brgoch, J. in Comprehensive Inorganic Chemistry III 3rd edn (eds Reedijk, J. & Poeppelmeier, K. R) 262–307 (Elsevier, 2023).
- 104. Hermus, M., Phan, P.-C., Duke, A. C. & Brgoch, J. Tunable optical properties and increased thermal quenching in the blue-emitting phosphor series: Ba₂(Y_{1-x}Lu_x)₅B₅O₁₇:Ce³⁺ (x = 0 - 1). Chem. Mater. 29, 5267-5275 (2017).

Acknowledgements

S.H., M.S. and J.B. thank the National Science Foundation (CER-1911311 and DMR-1847701) for supporting this work.

Author contributions

S.H. and M.S. researched data for the article. S.H., A.S. and J.B. contributed substantially to discussion of the content. S.H., M.S. and J.B. wrote the article. All authors reviewed and/or edited the manuscript before submission.

Competing interests

The authors declare no competing interests.

Additional information

Peer review information *Nature Reviews Materials* thanks Kee-Sun Sohn, Ru-Shi Liu and the other, anonymous, reviewer(s) for their contribution to the peer review of this work.

Publisher's note Springer Nature remains neutral with regard to jurisdictional claims in published maps and institutional affiliations.

Springer Nature or its licensor (e.g. a society or other partner) holds exclusive rights to this article under a publishing agreement with the author(s) or other rightsholder(s); author self-archiving of the accepted manuscript version of this article is solely governed by the terms of such publishing agreement and applicable law.

© Springer Nature Limited 2023